THE JOURNAL OF PHYSICAL CHEMISTRY A

Article

pubs.acs.org/JPCA

OH-Initiated Reactions of *p*-Coumaryl Alcohol Relevant to the Lignin Pyrolysis. Part I. Potential Energy Surface Analysis[⊥]

Rubik Asatryan,[*,†] Jason M. Hudzik,[‡] Joseph W. Bozzelli,[‡] Lavrent Khachatryan,[§] and Eli Ruckenstein[†]

[†]Department of Chemical and Biological Engineering, University at Buffalo, The State University of New York, Buffalo, New York 14226, United States

[‡]Department of Chemistry and Environmental Science, New Jersey Institute of Technology, Newark, New Jersey 07102, United States

[§]Department of Chemistry, Louisiana State University, Baton Rouge, Louisiana 70803, United States

Supporting Information

ABSTRACT: Cinnamyl alcohols such as *p*-coumaryl alcohol (*p*-CMA) are lignin models and precursors (monolignols) and the most important primary products of lignin pyrolysis. However, the detection of monomers is not straightforward since they either undergo secondary transformations or repolymerize to contribute to the char formation. Both concerted-molecular and free-radical pathways are involved in these processes. Our recent fundamentally based theoretical and low-temperature matrix-isolation−EPR studies of cinnamyl alcohols highlighted the role of side-chain reactivity in diversity of pyrolysis products and provided a network of the chemically activated H + *p*-CMA reactions (Asatryan et al. *J. Phys. Chem. A*, **2017**, *121*, 3352−3371). The readily available hydroxyl radicals also can trigger a cascade of free-radical processes. Here, we present a comprehensive potential energy surface (PES) analysis of the OH + *p*-CMA reaction using various DFT and *ab initio* protocols. Since the *p*-CMA involves both an alkyl OH-group and a side-chain double bond, the title reaction can also serve as a relevant model for reactions of unsaturated alcohols with hydroxyl radicals to form various oxygenates including polyhydric alcohols which are abundant in nature. The newly identified pathways suggest certain alternatives to the known radical reactions. Of particular interests are the roaming-like low-energy dehydration reactions to generate a variety of O- and C-centered intermediate radicals, which are mostly transformed into the phenolic compounds observed in pyrolysis experiments. Some concerted unimolecular decomposition pathways for *p*-CMA are also revealed, not considered previously, such as the migration of terminal OH-group, and/or it is splitting over the *ipso*-C and *ortho*-C atoms of the benzene ring to form bicyclic oxispiro- and chromene compounds represented in natural lignin.

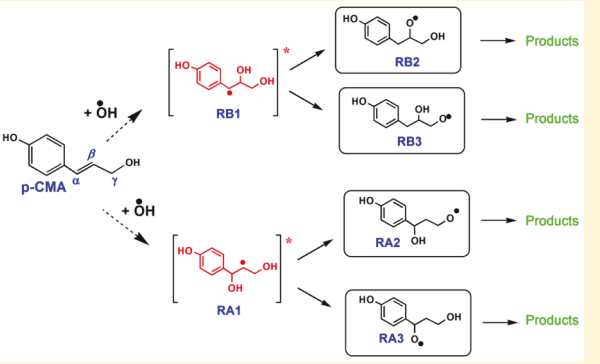

1. INTRODUCTION

Lignin is the second most prevalent biopolymer on Earth next to cellulose, and it accounts for almost 30% of the organic carbon in the biosphere.[1−12] It is an important resource of renewable fuels and their derivative high-value chemicals and is the main renewable feedstock for the industrial production of aromatic compounds.[2−7] However, the structural diversity and heterogeneity of lignin, along with its hydrophobic nature and insolubility in aqueous systems, pose challenges to controlled destruction of biomass to produce feedstock materials.[5,8]

Lignin is a three-dimensional, highly cross-linked macromolecule produced by radical polymerization of three phenylpropanoid monomers (monolignols) *cinnamyl alcohol* derivatives: *p*-coumaryl alcohol (*p*-CMA), coniferyl alcohol, and sinapyl alcohol, containing *p*-hydroxyl and *m*-methoxy groups on the rings[9−11] (Figure 1). The monomeric units in lignin macromolecules are engaged into a complex network

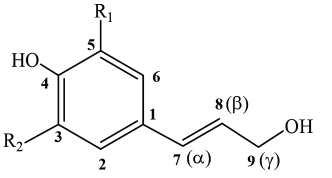

Figure 1. Chemical structure of monolignols: R_1 = R_2 = H for *p*-coumaryl alcohol (*p*-CMA), R_1 = H, R_2 = OCH_3 for coniferyl alcohol, and R_1 = R_2 = OCH_3 for sinapyl alcohol. Cinnamyl alcohol (CnA) contains no ring substituents. Allyl alcohol (AA) contains no ring.

Received: January 8, 2019
Revised: March 5, 2019
Published: March 8, 2019

DOI: 10.1021/acs.jpca.9b00185
J. Phys. Chem. A XXXX, XXX, XXX−XXX

through different types of ether and carbon−carbon bonds: β-O-4, α-O-4, 4-O-5, 5−5, β−β, benzodioxocin, and spirodienone.[2,6,8,9]

Pyrolysis of lignin is a key approach to produce low-molecular, primarily phenolic compounds.[7,12−28] A significant effort has been devoted to the pyrolysis mechanisms of lignin model compounds.[12,24−61] Most of the mechanistic information is deduced from thermal conversions of dimers comprised of the most abundant β-O-4 and α-O-4 aryl ether linkages in lignin (see, e.g., refs 24−27 and 29−43). The pyrolysis of monolignols, however, only recently became a focus of attention, even though the monomers have been known to be the most important primary products of the lignin pyrolysis.[22,49−61]

Several comprehensive and fundamental theory-based mechanistic and kinetic studies are also known on pyrolysis of the contracted, smaller models such as anisole,[62−66] catechol,[67,68] *o*-quinone methide[69−74] (*o*-QM), and chroman,[70,75] which are believed to be the key intermediates in lignin thermolysis and char formation (see also ref 41.).

This work continues our previous fundamentally based exploration of the pyrolysis mechanisms of lignin and its simple models—monolignols.[7,14,55−57] Here, the reactivity of the key monolignol *p*-CMA is examined toward hydroxyl radicals, which are produced in a pyrolysis reaction environment[22,55] in order to gain insight into the side-chain reactivity of lignin and its model compounds. A detailed potential energy surface (PES) analysis of the OH + *p*-CMA reaction is performed and compared with previous results on the reduction of the double bond in chemically activated H + *p*-CMA reactions.[55]

The *p*-coumaryl alcohol (*p*-CMA, Figure 1) is the simplest lignin model containing both phenolic hydroxyl group and hydroxypropenyl side-group (allyl alcohol moiety −CH=CHCH$_2$OH) of the cinnamyl alcohol backbone. The combination of an alkyl hydroxyl and double bond moieties separated by a methylene linkage is also a characteristic feature of the lignols and many lignin streams and renewable lignin feedstocks. Thus, the OH + *p*-CMA reaction can serve as a relevant model to examine the mechanistic impacts of side-chains on lignin thermolysis. Below we present a brief summary of related work relevant to our current analysis of *p*-CMA reactivity.

1.1. Lignin Pyrolysis. Dimer Models. Two *general mechanisms* have been proposed to operate during pyrolysis of lignin and its model compounds: (i) unimolecular concerted reactions, which primarily involve Maccoll and retroene pericyclic intramolecular type rearrangements, and (ii) radical processes initiated by homolytic bond cleavage followed by secondary bimolecular and isomerization reactions.[12,29,31,55−57,76−82] These mechanisms are dominating at different pyrolysis conditions. For the pure gas-phase processes, the two mechanisms are discriminated by temperature. For instance, Jarvis et al. suggested based on the detailed computational and experimental analysis of rate constants for pyrolysis of phenethyl phenyl ether model that the concerted mechanism dominates at typical dimer model pyrolysis temperatures of 500−600 °C, whereas the C−O aryl ether bond homolysis occurs at temperatures higher than 1000 °C.[29] However, the *depolymerization* of lignin is highly challenging due to its heterogeneity. There is also a recondensation tendency, often to form diverse species with *novel functionalities*,[4,18,72,83] which increases the role of the side groups in lignin pyrolysis. Moreover, the side groups constitute a considerable portion of the lignols and lignans (with two OH groups separated by two methyl linkages), and other models and derivatives of lignin.

It should be emphasized that the presence of the *functional groups* significantly affects the overall decomposition features and distribution of products in pyrolysis of lignin and model compounds.[12,17,22,84,85] The etheric bond fission is particularly sensitive to the substituents both in the side-chains and aromatic rings. The enlargement of the alkyl chain or addition of other electron donating groups, such as methylene and methoxy groups, enhances the thermal degradation of the dibenzyl ether (DBE) model, whereas the electron withdrawing groups, like aldehydes, decrease the reactivity of DBE.[19,84,85]

Free radical intermediates have been detected during the pyrolysis of lignin and its model compounds under various conditions: in the gas phase,[7,15] in bio-oil,[10,16] and in biochar media.[11] Kibet et al.[7] have particularly identified phenoxy and substituted phenoxy radicals in the gas phase from lignin pyrolysis at 450 °C using an *in situ* technique of low temperature matrix isolation in conjunction with electron paramagnetic resonance spectroscopy (LTMI-EPR).[86] It is common to consider the low temperatures operation of *radical processes* during lignin pyrolysis, in spite of the high characteristic bond dissociation energies (BDE) determined in model compounds; BDE for most abundant β-O-4 ether linkages is ca. 60 kcal/mol, and only for α-O-4 linkages they are somewhat lower (40−60 kcal/mol), whereas the reactive O−CH$_3$ bond cleavage requires 56.3 kcal/mol energy.[22] Since the primary lignin pyrolysis ranges from as low as 200−400 °C,[22] the additional factors such as heterogeneous processes may also well contribute to the initiation of radical processes. The fractional pyrolysis employed in our recent study,[55] could serve as a relevant example.

Dehydration is a key process in pyrolysis; however, there is little knowledge on its diversity. Dehydration can simply occur via direct H-abstraction by OH radicals or OH-abstraction by H atoms; however, such bimolecular reactions can occur at relatively higher temperatures, as shown by Zhang et al. for OH + allyl alcohol reaction based on kinetics calculations[87] (*vide infra*). However, the low-energy pathways can be provided by the chemically activated processes involving a roaming pathway[88] (*vide infra*), as well as the *heterogeneous* catalytic processes mediated by solid residues.

To explain degradation of macromolecular structures (linkages), the dimer models of lignin are most extensively studied (see, e.g., refs 24−27, 29−40, 42, and 77−82), whereas the mechanisms and kinetics of the monolignols' decomposition are less explored.

1.2. Pyrolysis of Monomers. Strong interest has been raised in recent years concerning the pyrolysis of monolignols.[43−61] The *direct* mass-spectrometric analysis of pyrolyzates from wood and isolated lignin suggested that the monomeric cinnamyl alcohols, such as coniferyl alcohol and sinapyl alcohol, are the most important *primary* products in lignin pyrolysis.[18,22] However, the higher reactivity of monomers typically prevents detection of significant amounts of monolignols during lignin pyrolysis.

Quite similar to natural lignin, pyrolyzates have been found in pyrolysis products of coniferyl alcohol, *viz.*, coniferyl aldehyde (an oxidation product), dihydroconiferyl, and isoeugenol (reduction products), as well as *cis*-coniferyl alcohol and 4-vinylguaiacol associated with the side chain conversion

DOI: 10.1021/acs.jpca.9b00185
J. Phys. Chem. A XXXX, XXX, XXX−XXX

products.[22,53] The cinnamyl alcohol end groups in lignin have also been suggested to contribute to the formation of propenylphenols and cinnamyl compounds (dihydrocinnamyl alcohol, cinnamaldehydes, and cinnamyl alcohol (CnA)) in lignin pyrolysis.[49,54]

Unlike dimers, the pyrolysis mechanisms of isolated monolignols are not well explored and most of the proposed product-formation channels are postulated based on indirect information.[22,50−54,59,60] The secondary transformations of monolignols (primarily, the side-chain conversions and repolymerization[4,18,22,53]) are also believed to involve both concerted-molecular and free-radical mechanisms.[12,22,53,55−57]

Our recent LTMI-EPR experiments combined with detailed PES analysis provided fundamentally based reaction pathways for pyrolysis of cinnamyl alcohols and, in particular, suggested the side-chain reactivity as the key factor in diversity of the pyrolysis products.[40,42,55−57] A combined radical-molecular mechanism explained the primary products formation during pyrolysis of the *p*-CMA and cinnamyl alcohol (CnA)—the simplest model of lignols, involving no *p*-hydroxyl group.[56]

The radical-species have been registered in our *in situ* experiments using cryogenic-EPR detection technique during pyrolysis of CnA[55,56,86] and *p*-CMA.[55,57] Based on the comparisons of experimental and theoretical *g*-tensors of the model structures, it was concluded that the complex mixtures of the detected open-shell intermediates mainly consist of *O-centered* and *O-linked* conjugated delocalized radicals.[56]

A mechanistic analysis has also been performed for medium and high temperature range (400−900 °C) pyrolysis of cinnamyl alcohol. DFT analysis particularly suggested that the major products indene, styrene, benzaldehyde, 1-propynyl benzene, and 2-propenyl benzene are formed via simple bond dissociation, which are dominant at high temperatures, and some other unimolecular decomposition pathways, such as dehydrogenation, dehydration, 1,3-sigmatropic H-migration, 1,2-hydrogen shift, C−O and C−C bond cleavage processes.[56] Mainly phenolic compounds (phenol, *p*-cresol, ethyl-, propenyl-, and propylphenols) were identified in molecular products of our recent *fractional* pyrolysis experiments on *p*-CMA, predominantly formed at low temperatures (e.g., ca. 74% at 350 °C). DFT-analysis suggested plausible decomposition pathways involving highly conjugated aromatic and simple radicals.[55] The dominant formation of phenolics is in full accordance with available experimental data by Akazawa et al.,[12,22,59−61] who also hypothesized a basic reaction mechanism primarily involving the homolytic bond cleavage and H-abstraction reactions that may in principle occur by H atoms and OH radicals.

Three primary decomposition pathways of *p*-CMA have been studied by Furutani from DFT-analysis and rate constants evaluation.[61] They involved C(8)−C(9) and O(9)-H bond cleavages, and H-addition to C_β-atom followed by C(8)−C(9) bond fission in the formed adduct. Two H-abstraction reactions from terminal OH-group by H and CH_3- radicals have also been evaluated.

1.3. Reactivity of the H-Atoms and OH-Radicals toward Monomers. The H atom and OH radicals are readily formed in the pyrolysis environment which can reduce side-chain double bonds[22,40,42,55] and abstract H atoms and functional groups. Several reaction channels have been suggested to regenerate the radicals[22,55] including the ones we identified relevant to the pyrolysis of *p*-CMA and cinnamyl alcohol.[55−57]

One of the identified pathways acting as a source of H atoms and involving *β*-scission reactions converting $^{\bullet}C_\gamma$−OH radical to C_γ=O (in coniferyl aldehyde)[55] agrees well with what was suggested by Kawamoto based on the chemical intuition.[22] The possible H-abstraction reactions have largely been evoked to postulate various mechanisms for decomposition of lignols and other lignin models.[22,42,60,61] A detailed PES analysis demonstrated an essential role of the chemically activated processes triggered by H-addition to the double bond of *p*-CMA to major molecular products,[55] including various dihydro- derivatives, such as dihydrocinnamyl and other aldehydes, as well as hydrogenated monolignols.

1.3.1. OH-Addition. The smallest relevant model of the OH radical reaction with unsaturated alcohols, such as monolignols, is OH + allyl alcohol (AA, CH_2=$CHCH_2OH$) reaction[87−92] where AA reproduces the propanoid side-chain of the monolignols. The chemically activated model reaction OH + AA has been studied experimentally extensively[89−92] as well as a few theoretical studies.[87,88,92]

Various isomerization and unimolecular decomposition channels have been identified in the most recent and comprehensive theoretical study by Zhang et al. at the G2MP2//MP2/6-311++(d,p) level of theory.[87] It involves formation and decomposition of two chemically activated 1,3- and 1,2-diol radical adducts (***1,3-DR*** and ***1,2-DR*** respectively; the notations come from ref 88). Nevertheless, the simple bond cleavages in intermediate radicals were found to be the most affordable reactions. The water elimination also was simply evaluated via bimolecular (direct) H-abstraction reactions involving four available types of H atoms bound to the C1, C2, C3, and O atoms, respectively, to form CH_2=$CHCH_2O^{\bullet}$, CH_2=$CHC^{\bullet}HOH$, CH_2=$C^{\bullet}CH_2OH$, and $C^{\bullet}H$=$CHCH_2OH$ intermediate radicals. However, the possible dehydration reactions of the energized radical-adducts have not been explored. It is important to note that the kinetics analysis by Zhang et al.[87] predicted that even the most feasible direct (bimolecular) dehydration channel involving H-abstraction at C(1)-position of AA to form the most stable *α*-hydroxy radical, becomes dominant only at high temperatures, whereas the radical addition-adduct $CH_2{}^{\bullet}CH(OH)$-CH_2OH (***1,2-DR***) formed from collisional stabilization prevails at 200−400 K temperatures and atmospheric pressure (being, notably, a typical condition for lignin primary pyrolysis, *vide supra*).

On the other hand, a quite recent PES analysis of OH + AA reaction revealed[88] the low-energy unimolecular dehydration channels for ***1,2-*** and ***1,3-DRs*** chemically activated intermediates, which can be well interpreted as *roaming* processes. The roaming features attributed to the OH + AA reaction are (a) "loose" transition state geometries involving an almost dissociated hydroxyl group, (b) the energies very close to the (OH + AA) asymptote, (c) a characteristic low imaginary frequency mode (100−200 cm^{-1}) along the reaction coordinate, and (d) the flatness of the roaming region of the PES which is the most important feature of the roaming phenomenon.[88,93−96] These are in line with a simpler dehydration[55−57] reaction of C_2H_4OH radical-adduct where the roaming has been strongly proven to contribute based on a series of comprehensive photochemical and theoretical studies.[97,98] Closely related roaming phenomena have also been claimed recently to occur in some larger systems[99] and in the condensed phase.[100]

DOI: 10.1021/acs.jpca.9b00185
J. Phys. Chem. A XXXX, XXX, XXX−XXX

Scheme 1. Reaction Pathways Triggered by OH− Addition to the C7(α)- and C8(β)-Atoms of the Double Bond in *p*-CMA, Calculated at the ωB97X-D/def2TZVP Level[a]

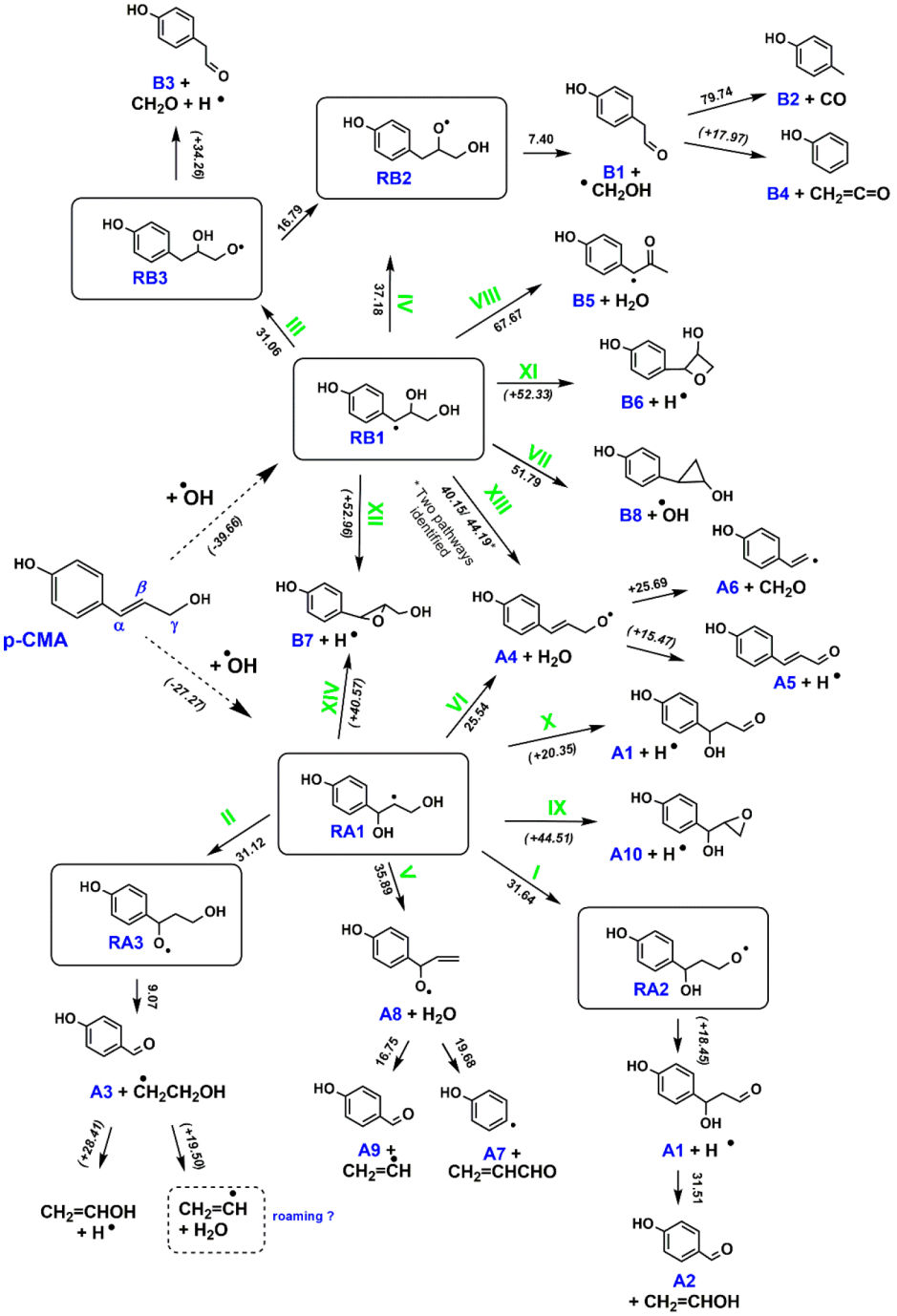

[a]Data on arrows represent corresponding barrier heights (ZPE-corrected electronic energies) or dissociation limits (in italic and parentheses) in kcal/mol. Reaction channel (*ch*N) notation is given in Roman numerals (for N). Channels VI (via ***TSa5***) and XIII (via ***TSb8***) represent the roaming pathways along with dissociation of CH_2CH_2OH (see text).

Whereas the rate coefficients of the OH + unsaturated alcohol reactions are only weekly dependent on the chain length of the alcohol,[101] the structure of the side chain plays a decisive role As shown by Bruycker et al.[38] based on the reactivity of prenol and isoprenol containing a C═C double bond in the β-and γ-positions to the hydroxyl group in pyrolysis and oxidation processes.

To conclude, despite significant achievements in lignin pyrolysis, the knowledge of elementary reaction mechanisms, even in case of the simple precursors and model compounds, remains limited. The fundamentally based mechanistic studies are therefore essential in progressing development of the novel pathways and comprehensive kinetic schemes.

The paper at hand provides detailed analysis of the chemically activated reactions of *p*-CMA with OH-radicals. A detailed PES analysis is performed for reaction of OH-radicals with the side-chain double bond of *p*-CMA. A detailed kinetics

DOI: 10.1021/acs.jpca.9b00185
J. Phys. Chem. A XXXX, XXX, XXX−XXX

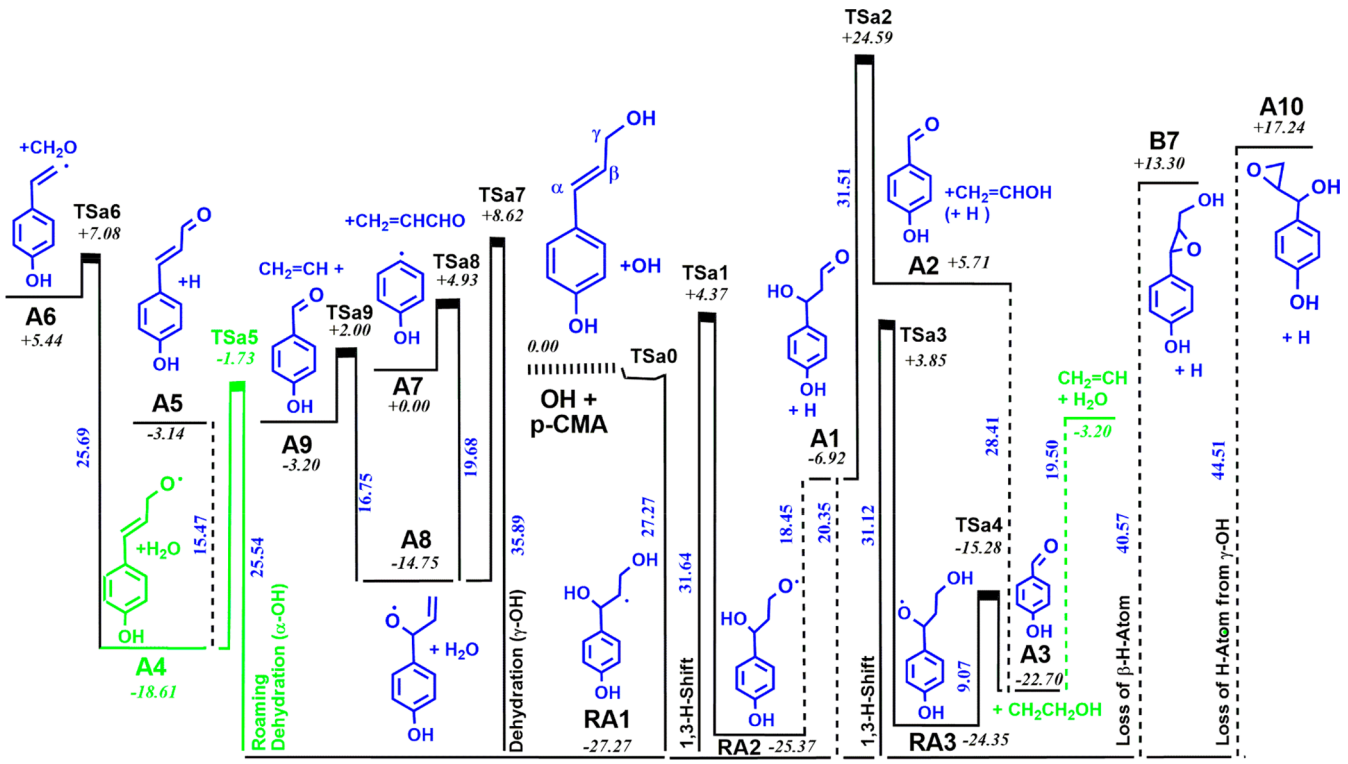

Figure 2. Energy diagram (kcal/mol, ZPE-corrected electronic energies) for OH-addition to the C7(α)-center of the side chain double bond in *p*-CMA (Figure 1). The roaming-related pathways are highlighted in green. Note that species ***A2***, ***A3***, and ***A9*** are identical but are labeled separately in the figure for clarity.

analysis will be provided separately as a second part of this study.

The *H-abstraction* of phenolic hydroxyl groups typically initiates formation of the quinoidal intermediates and conjugated products[22,41,55,70,73] as we also recently demonstrated during the pyrolysis of monolignols.[55−57] Thus, the unique reactivity of the O-bound H atoms in phenolic OH-groups supporting the production of polyaromatics and the solid residues will not be considered further in this paper (see also section 3.2), which is mainly aimed to explain phenolic compounds observed in our experiments.

Section 2 provides calculation details. A detailed analysis of the PES for OH + *p*-CMA reaction is described in section 3. Since the various concerted unimolecular decomposition and radical reactions of *p*-CMA (as well as its truncated version CnA) were previously explored,[55−57] our efforts will be more focused on the exploration of PES for addition−elimination (chemical activation) reactions triggered by OH-addition to the double bond. We examined the possible formation reactions of product-radicals, involving also dehydration of DR-adducts, in particular, the possibility of the roaming-like mechanisms, which we have quite recently suggested to occur with the diol radicals.[88]

2. CALCULATION METHODS

Various decomposition pathways of OH + *p*-CMA reactions and relevant intermediates are computed using nonlocal Kohn−Sham density functional theory based on the generalized gradient approximation.[102] A detailed screening of PES is performed at ωB97XD/6-31+G(d,p) level of theory, which involves ωB97XD dispersion- and long-range corrected hybrid method[103] in conjunction with the moderate Pople-type basis set 6-31+G(d,p) augmented with diffuse and polarization functions.[104,105] The stationary points are recalculated using the extended def2TZVP basis set[106] with the final optimized geometries reported in the Supporting Information from the ωB97XD/def2TZVP level of theory.

In addition, the well depths of the OH-addition to the double bond of *p*-CMA are re-evaluated using other DFT functionals, such as the popular M06-2X[107] and B3LYP[108,109] methods, for comparison. Notably, the well depths predicted by M06-2X/6-31+G(d,p) method coincides with those obtained at ωB97XD/6-31+G(d,p) level using the same basis set (42.2 and 31.1 kcal/mol vs 42.1 and 30.7 kcal/mol, respectively). The barrier heights calculated at M06-2X and ωB97XD levels are also fairly close to each other (section 3.1). Calculations for unimolecular decomposition of *p*-CMA are performed using B3PW91 hybrid method in conjunction with minimally augmented 6-31+(2d,p) basis set to be comparable with related results from our previous study.[55]

All employed methods are well tested in literature in the same domain, including our previous studies on the various open-shell and molecular systems.[80,104,110−116] The minimally augmented basis set (cf. Karlsruhe def2-SVP or ma-SVP), has been recommended by Truhlar et al. as the best affordable basis set for exploration of reaction barriers in large molecular systems.[104] Notably, the same ωB97XD/6-31+G(d,p) method has been successfully utilized recently for evaluation of the PES for dissociation of C_2H_5 radical to C_2H_3+H_2 products involving the *roaming* dynamics, in accord with QCISD(T) data.[114]

Transition states are characterized as having only one negative eigenvalue of Hessian (force constant) matrices. The absence of imaginary frequencies verifies that structures are true minima at their respective levels of theory. The intrinsic

DOI: 10.1021/acs.jpca.9b00185
J. Phys. Chem. A XXXX, XXX, XXX−XXX

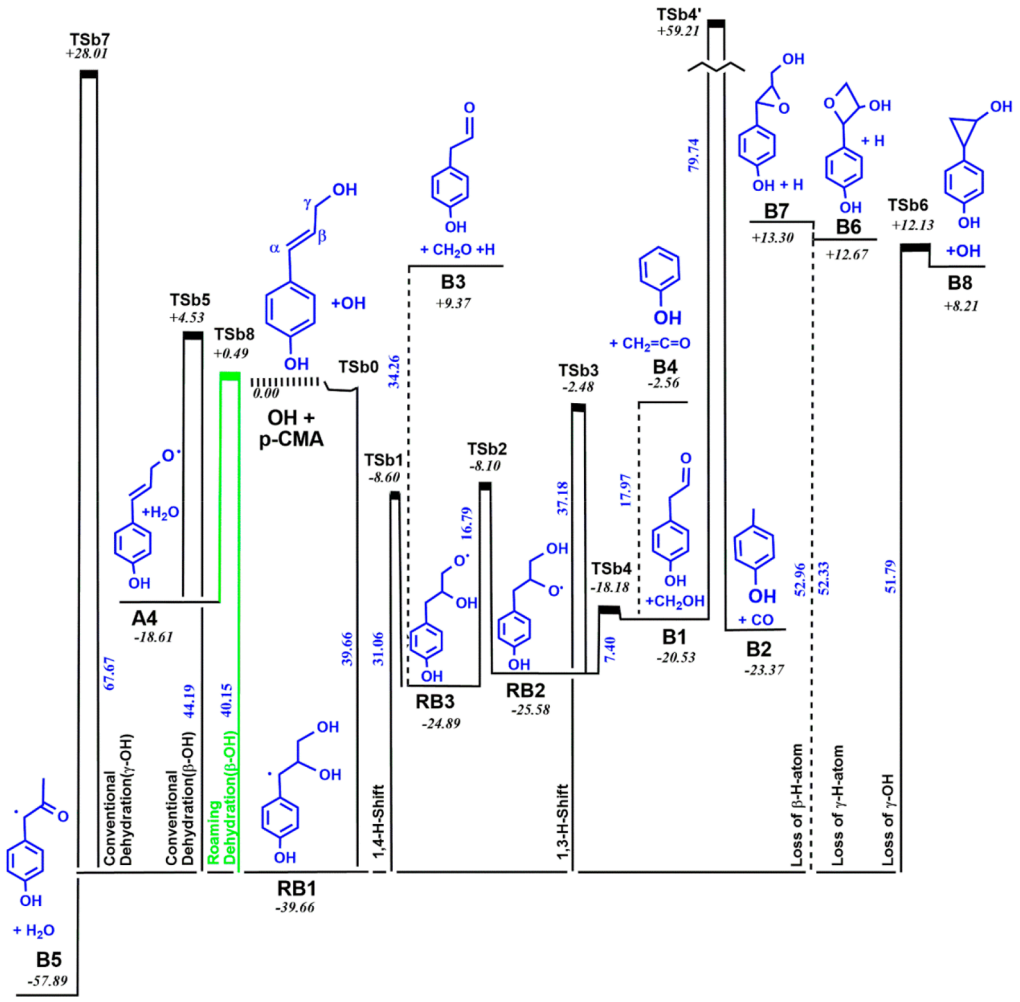

Figure 3. Energy diagram (kcal/mol, ZPE-corrected electronic energies) for OH-addition to the C8(β)-center of the side chain double bond in *p*-CMA (Figure 1). The roaming-related pathway is highlighted in green. Note that species ***B1*** and ***B3*** are identical but are labeled separately in the figure for clarity.

reaction coordinate (IRC) analysis is performed at ωB97XD/def2TZVP level. All PES calculations are performed using the Gaussian 16 program (Revision A.03).[117]

3. RESULTS AND DISCUSSION

3.1. Addition of OH-Radicals to the Double Bond. The addition of hydroxyl radical to a double bond is a straightforward process, which generally occurs without any barrier of activation; however, some small decomposition barriers arise when a prereaction complex is formed (see, e.g., ref 88.).

The OH-addition can occur also at the *ipso*-carbon position of the benzene-ring, which as we demonstrated earlier for catechol pyrolysis,[67,68] would provide options for formation of ring-opening products such as dienones (see also ref 118.). However, we did not consider this option here applied to the *p*-CMA pyrolysis since the aromatic ring is preserved in the major products, phenolics, for our pyrolysis conditions.[55] The same also occurs for coniferyl alcohol at primary pyrolysis temperatures, reported by Kawamoto et al.,[53] as well as other monomers, including *p*-CMA, even at higher 600 °C temperatures.[59]

The addition of OH-radical to a double bond generates chemically activated adduct-radicals which can further isomerize and decompose to form products (see, e.g. refs 38, 88, 112, 115, and 119). The stabilization of energized adducts can be a path to the formation of widespread polyhydric alcohols found in nature.

Scheme 1 illustrates a network of reactions triggered by OH-addition to the double bond of the *p*-CMA with corresponding energetic diagrams, which include zero-point vibrational energies (ZPE) corrected electronic energies from ωB97XD/def2TZVP calculations, in Figures 2 and 3. Structures of the reagents, products, and transition states in this analysis are shown in Figure 4.

As seen in Figures 2 and 3, the addition of OH-radical to the C_β atom (C8 in Figure 1) forms chemically activated ***RB1*** adduct, which is thermodynamically preferred (more exothermic) by ca. 12 kcal/mol compared to the C_α addition adduct ***RA1***. Such a preference correlates with charge distribution in *p*-CMA calculated both at single point CCSD(T)/6-31G(d,p)//ωB97XD/6-31+(2d,p) and optimized MP2/6-31+(d,p) levels. As a strong electrophile, the $^{\bullet}$OH radical is expected to prefer to add at the electron-rich C8 site of the *p*-CMA molecule (MP2 data in parentheses): q(C8) = −0.16 (−0.15) e vs q(C7) = −0.10 (−0.11) e. The site-selective OH-addition to the aromatic ring is a classic example of such correlation.[118]

DOI: 10.1021/acs.jpca.9b00185
J. Phys. Chem. A XXXX, XXX, XXX−XXX

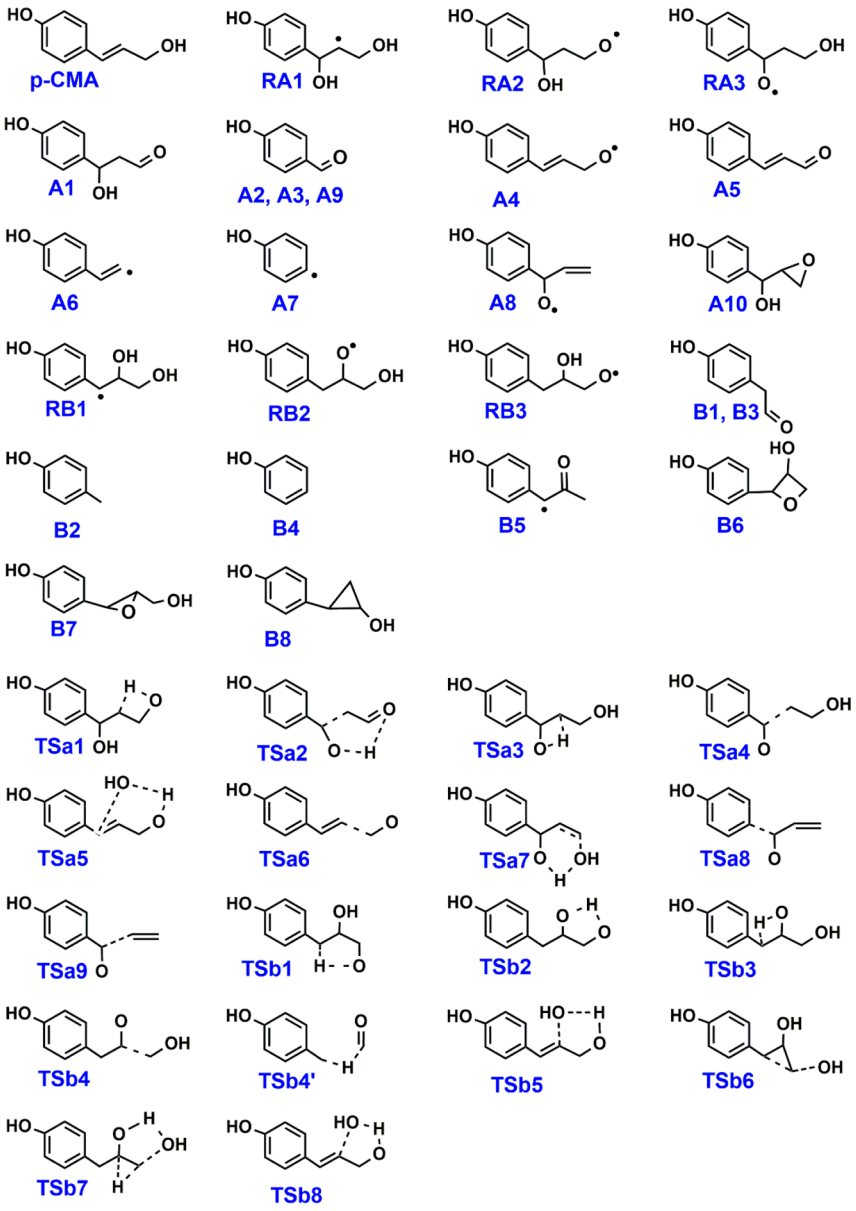

Figure 4. Structures of reagents, products, and transition states.

The preferred C8 addition seems to correlate also with spin distribution in the generated diol radicals (DR). The increased *delocalization* of the spin density is known to correlate with stability of the intermediate radicals (explaining, particularly, the propagation steps in the radical polymerization processes[120] (more details are provided in ref 56). As expected, in both diol radicals the unpaired electron is mostly localized in the reaction centers: ρ(C8) = 0.95 e, ρ(C7) = 0.73 e, respectively for 1,2-DR (***RB1***) and 1,3-DR (***RA1***) adduct radicals. Considering that more spin is delocalized (less localized) the more stable the formed radical is, the 1,2-DR with lower spin density of 0.73e is predicted to be more stable, as seen in Figures 2 and 3.

The same preferences are also seen for the model reaction OH + allyl alcohol ($C_\beta H_2{=}C_\alpha H{-}CH_2OH$), where no electron-rich and bulky hydroxy-phenyl substituent is present at C_β position.

The OH radical in the model reaction prefers attacking the less-substituted carbon-center (Markovnikov-like addition) corresponding to the C(8,β) position in *p*-CMA to form the 1,2-diol radical.

The well depths for OH + AA reaction are 29.0 kcal/mol vs 30.5 kcal/mol, respectively, for OH-addition to C_γ (to form 1,3-DR) and C_β (to form 1,2-DR) atoms, calculated at CCSD(T) // UB97D3 level of theory,[88] versus 27.3 and 39.7 kcal/mol, respectively, in *p*-CMA (Figures 2 and 3).

Perhaps, the electronical effects and steric interactions are not the only reasons for this, rather it can also be attributed to the formation of the H-bonding between vicinal OH-groups providing additional stabilization of the 1,2-DRs, as opposed to the 1,3-DRs with further separated hydroxyl groups. This is seen in the ωB97XD/def2TZVP optimized geometry bond distances. For ***RA1***, the bond distance is 2.07 Å as measured from the hydrogen atom of the C_γ−OH to the oxygen atom of the C_α−OH group. A longer distance of 2.34 Å is seen in the ***RB1*** bond length between the hydrogen atom of the C_γ−OH and the oxygen atom of the C_β−OH group

DOI: 10.1021/acs.jpca.9b00185
J. Phys. Chem. A XXXX, XXX, XXX−XXX

It is interesting also to note that the well depths evaluated with the ωB97XD/6-31+G(d,p) method are almost identical to those calculated with M06-2X using the same minimally augmented basis set (*viz.,* 42.0 and 30.7 kcal/mol (ωB97XD) for ***RB1*** and ***RA1*** adducts, respectively, versus 42.2 and 31.1 kcal/mol (M06-2X)). Such a perfect consistency increases the credibility of both methods for such reactions.

It is important to note that the B3LYP/6-31+G(d,p) method also predicts almost the same energy difference of ca. 10 kcal/mol between the ***RA1*** and ***RB1*** adducts, albeit the absolute values of well-depths differ significantly (42.0 and 30.7 kcal/mol (ωB97XD) vs 32.8 and 22.3 kcal/mol (B3LYP), respectively) Perhaps this is due to some underestimation of radical-adducts' energy at B3LYP level. The single point CCSD(T) calculations support the energy difference obtained at dispersion-and-long-range-corrected ωB97XD level (not provided here).

As seen from the energetic diagrams illustrated in Figures 2 and 3, further isomerization and decomposition of energized adducts chemically activated by OH-addition are rather affordable and can serve as important product formation channels. The major reaction channels (*ch*N) are identified in this work using the Roman numeral notation for N in Scheme 1 for clarity. In the following analysis and discussion, these channels are referenced as well as the relative energy barriers calculated from the ωB97XD/def2TZVP level of theory. It is also important to note that species ***A2***, ***A3***, and ***A9*** are identical as seen in Figure 4, but are labeled separately for clarity in Figures 2 and 3. The same holds for species ***B1*** and ***B3*** in these figures. Finally, species ***A4*** is the same as a key radical intermediate, ***R(09)***, identified in our previous H + *p*-CMA study.[55] Only the ***A4*** notation will be used here for clarity.

3.1.1. Formation of Pre- and Post-Reaction van der Waals (VdW) Complexes. Some results are provided for the model OH + AA reaction reproducing the reactive side chain.[88] Formation of VdW-complexes are optimal situations for pool radicals, such as OH, to interact with the target species for periods of time allowing for potential H atom abstraction to generate a *p*-CMA radical, and for this analysis, water. Previously we determined that the flatness of the PES regions coupled with these VdW complexes, created situations which facilitated roaming dissociation. For OH + AA, the lowest dissociation pathways employed two interactions: the OH radical oxygen atom to the terminal hydroxyl group of AA along with OH radical hydrogen atom to AA π-bond.

3.1.2. C_α-Addition−Isomerization Reactions. The addition of OH-radical to the C_α atom of the double bond forms an energized adduct ***RA1*** (Figure 2 and eq 1) with a well depth of 27.27 kcal/mol. The energized ***RA1*** radical can be further isomerized to ***RA2*** radical-intermediate (*ch*I) via H-transfer from the γ-OH group through the barrier of ***TSa1*** of 31.64 kcal/mol height, which is only 4.37 kcal/mol higher than the energy of the free reactants (entrance level), which is used as a reference level. The ***RA2*** radical is approximately at the same well depth of ***RA1*** at −25.37 kcal/mol.

The loss of a H atom from the Cγ-position of ***RA2*** (eq 2) generates an α-hydroxy-isomer of cumaraldehyde (***A1***). This is an affordable channel ($\Delta E^{\#}$ = 18.45 kcal/mol based on the dissociation limit while still below the entrance level) also for regeneration of the reactive H atom. A secondary pathway to generate the products in eq 2 involves the straight dissociation from ***RA1*** (*ch*X). The barrier height of 20.35 kcal/mol, calculated from the dissociation limit, is comparable in magnitude to 18.45 kcal/mol from ***RA2***. The aldehydes are dominant products in pyrolysis of monomers in various conditions.[22,56,59]

The cinnamyl alcohol was also the major product of the CnA pyrolysis in our experiments in 400−900 °C temperature range conditions.[56]

The barrier height of 20.35 kcal/mol, calculated from the dissociation limit, is comparable in magnitude to 18.45 kcal/mol from ***RA2***. The aldehydes are dominant products in pyrolysis of monomers in various conditions.[22,56,59] The cinnamaldehyde was also the major product of the CnA pyrolysis in our experiments in 400−900 °C temperature range conditions.[56]

Figure 2 also shows a further decomposition pathway for ***A1*** via H-transfer of α-hydroxy group to the C_β radical center of ***RA1*** accompanied by C_α−C_β bond fusion. Surpassing the barrier height of 31.51 kcal/mol generates 4-hydroxybenzaldehyde (HOPhHCO, ***A2***) and vinyl alcohol (eq 3).

$$p\text{-CMA} + {}^{\bullet}\text{OH} \rightarrow \textbf{\textit{RA1}} \quad (1)$$

$$\textbf{\textit{RA1}} \rightarrow \textbf{\textit{RA2}} \rightarrow \text{HOPhCH(OH)CH}_2\text{CHO}\ (\textbf{\textit{A1}}) + {}^{\bullet}\text{H} \quad (2)$$

$$\text{HOPhCH(OH)CH}_2\text{CHO}\ (\textbf{\textit{A1}}) \rightarrow \text{HOPhHCO}\ (\textbf{\textit{A2}}) + \text{CH}_2{=}\text{CHOH} \quad (3)$$

The second isomerization channel (*ch*II) for the energized adduct ***RA1*** involves H-transfer of the α-hydroxy group to C_β to form ***RA3*** (eq 4) via a barrier of 31.12 kcal/mol. This barrier height is located approximately at the entrance channel level (only 3.85 kcal/mol higher), and thus is energetically accessible for the energized ***RA1*** adduct.

The newly generated ***RA3*** radical-intermediate provides a further affordable decomposition option (the ***TSa4*** structure creates a 9.07 kcal/mol barrier) through C_α-C_β bond fusion to form 4-hydroxybenzaldehyde (***A3***) and hydroxyethyl radical (eq 5). Note that ***A2*** is equivalent to the ***A3*** and ***A9*** structures. Further reaction of the generated ${}^{\bullet}\text{CH}_2$−CH_2OH radical could also lose a H atom to form vinyl alcohol over a 28.41 kcal/mol barrier (eq 6). The radical could also undergo a roaming dehydration, as suggested by Kamarchik et al.[97] relevant to the photochemical conditions (eq 7) with a dissociation limit barrier height of 19.50 kcal/mol.

$$\textbf{\textit{RA1}} \rightarrow \textbf{\textit{RA3}} \quad (4)$$

$$\textbf{\textit{RA3}} \rightarrow \text{HOPhHCO}\ (\textbf{\textit{A3}}) + {}^{\bullet}\text{CH}_2 - \text{CH}_2\text{OH} \quad (5)$$

$${}^{\bullet}\text{CH}_2 - \text{CH}_2\text{OH} \rightarrow \text{CH}_2{=}\text{CHOH} + {}^{\bullet}\text{H} \quad (6)$$

$${}^{\bullet}\text{CH}_2 - \text{CH}_2\text{OH} \rightarrow \text{CH}_2{=}\text{C}{}^{\bullet}\text{H} + \text{H}_2\text{O} \quad (7)$$

3.1.3. C_β-Addition−Isomerization Reactions. The addition of OH-radical to the C_β-atom of the double bond generates ***RB1*** energized adduct (Figure 3) with a well depth of 39.66 kcal/mol. This is a larger well depth than that for the C_α-addition due to the formation of intramolecular H-bonding between vicinal OH-groups.

The isomerization of ***RB1*** radical-adduct (*ch*III) via H-transfer of terminal γ-OH-group to C_α leads to the formation of ***RB3*** intermediate via a barrier height of 31.06 kcal mol^{-1} (Figure 3). This barrier energy is significantly lower (by 6.12 kcal/mol) than the 37.18 kcal/mol barrier for the isomerization to ***RB2*** (*ch*IV) via a H-transfer of β-OH group.

DOI: 10.1021/acs.jpca.9b00185
J. Phys. Chem. A XXXX, XXX, XXX−XXX

The H-transfer from the two OH-groups of the ***RA1*** to form ***RA2*** and ***RA3*** intermediates (Figure 2) occurs via energy barriers of similar magnitude (31.64 and 31.12 kcal/mol for channels I and II, respectively). H-transfer of the ***RB1*** radical to form ***RB3*** also has a similar barrier height of 31.06 kcal/mol (*ch*III) while transfer to form ***RB2*** is elevated at 37.18 kcal/mol (*ch*IV). The latter radical formation passes through a constrained four-member ring ***TSb3*** species, and although ***TSa1*** and ***TSa3*** both have similar cyclic TSs, the vicinal OH group provides a more unfavorable pathway. The same is seen with ***TSb1*** (for ***RB3*** formation) where there is a more favorable five-member ring structure, but still not a significant drop in the energy barrier compared to the transition states for ***RA1*** isomerization.

The loss of H at O8 to trigger further decomposition of the ***RB3*** intermediate via homolysis of the C8−C9 bond requires 34.26 kcal/mol energy and creates $HOPhCH_2CHO$ (***B3***). This ***RB3*** bond homolysis is favored entropically—it initiates formation of 4-hydroxyphenylacetaldehyde, formaldehyde, and spontaneously regenerates an H atom (eq 8).

$$\textbf{\textit{RB3}} \rightarrow HOPhCH_2CHO\ (\textbf{\textit{B3}}) + CH_2O + {}^{\bullet}H \quad (8)$$

On the other hand, an alternative more affordable pathway to form ***B3*** is via isomerization of ***RB3*** → ***RB2*** where the H-transfer faces only a 16.79 kcal/mol barrier.

A secondary barrier of lower energy at 7.40 kcal/mol for further elimination of the key ${}^{\bullet}CH_2OH$ radical from ***RB2*** and formation of $HOPhCH_2CHO$ (***B1***), as seen in eq 9, can further emphasize the role of this channel. Therefore, a combined channel of ***RB3*** → ***RB2*** → $HOPhCH_2CHO$ (***B1***) + ${}^{\bullet}CH_2OH$ (eq 10) can dominate over direct formation of ***B3*** from ***RB3*** (eq 8) with its 34.26 kcal/mol barrier height (note that ***B1*** is an equivalent structure to ***B3***).

$$\textbf{\textit{RB2}} \rightarrow HOPhCH_2CHO\ (\textbf{\textit{B1}}) + {}^{\bullet}CH_2OH \quad (9)$$

$$\textbf{\textit{RB3}} \rightarrow \textbf{\textit{RB2}} \rightarrow HOPhCH_2CHO\ (\textbf{\textit{B1}}) + {}^{\bullet}CH_2OH \quad (10)$$

Note the formation of important intermediate radical ${}^{\bullet}CH_2OH$.

The product ***B1*** can then undergo two further pathways as seen in Figure 3. One possibility is the loss of ketene leading to formation of phenol (***B4***) which has a barrier height of 17.97 kcal/mol calculated from the dissociation limit (eq 11). The secondary pathway for ***B1*** breakdown involves the terminal loss of carbon monoxide yielding *o*-cresol (***B2***) as the cyclic product (eq 12). This barrier is more than four times that of forming ketene and ***B4*** with an energy of 79.74 kcal/mol through ***TSb4′*** which is 59.21 kcal/mol above the entrance channel.

$$HOPhCH_2CHO\ (\textbf{\textit{B1}}) \rightarrow HOPh\ (\textbf{\textit{B4}}) + CH_2{=}C{=}O \quad (11)$$

$$HOPhCH_2CHO\ (\textbf{\textit{B1}}) \rightarrow HOPhCH_3\ (\textbf{\textit{B2}}) + CO \quad (12)$$

3.1.4. Dehydration Channels. The presence of two OH-groups in both separated and vicinal ***1,3-DR*** (***RA1***) and ***1,2-DR*** (***RB1***) types of radical-adducts provides opportunity for intramolecular isomerization reactions via larger TS-rings (and thus lower energy barriers). An important pathway is dehydration through interaction of two OH-groups. In general, four types of reactions can occur in this regard—two for each adduct: α/β-OH dissociates and abstracts H atom of the γ-OH group, and *vice versa,* an isolated γ-OH group abstracts an H atom from the α/β-OH group. In both types of adducts, the elimination of γ-OH and abstraction of the counterpart O-bound H atom occurs through a higher energy barrier since it produces an unstable product-radical.

In the case of the ***RB1***-adduct (*ch*VIII, eq 13), such dehydration is accompanied by a concomitant intramolecular H-shift to stabilize the product $HOPhCH^{\bullet}C(=O)CH_3$ (***B5***), which creates a prohibitively high barrier (67.67 kcal/mol, Figure 3). The initial rotation of the CC−CC dihedral angle and formation of *cis*-isomer increases the barrier by 2 kcal/mol.

$$\textbf{\textit{RB1}} \rightarrow HOPhCH^{\bullet}C(=O)CH_3\ (\textbf{\textit{B5}}) + H_2O \quad (13)$$

No rearrangement is needed for dehydration of the ***RA1***-adduct (*ch*V, eq 14) hence a lower-barrier of 35.89 kcal/mol is calculated to form an O-centered intermediate radical ***A8***: $HOPhCH(O^{\bullet})CH{=}CH_2$. The barrier is only 8.62 kcal/mol higher (***TSa7***) than the entrance channel and can likely occur in a medium temperature range.

$$\textbf{\textit{RA1}} \rightarrow HOPhCH(O^{\bullet})CH{=}CH_2\ (\textbf{\textit{A8}}) + H_2O \quad (14)$$

Decomposition of the $HOPhCH(O^{\bullet})CH{=}CH_2$ (***A8***) radical intermediate from eq 14 over a 19.68 kcal/mol energy barrier forms acrolein and generates *para*-hydroxy phenyl radical $HOPh^{\bullet}$ (eq 15). A competing decomposition reaction (eq 16) can also occur, forming 4-hydroxphenylacetaldehyde and vinyl radical over a slightly lower energy barrier of 16.75 kcal/mol.

$$HOPhCH(O^{\bullet})CH{=}CH_2\ (\textbf{\textit{A8}}) \rightarrow HOPh^{\bullet}\ (\textbf{\textit{A7}}) + CH_2{=}CHCHO \quad (15)$$

$$HOPhCH(O^{\bullet})CH{=}CH_2\ (\textbf{\textit{A8}}) \rightarrow HOPhHCO\ (\textbf{\textit{A9}}) + CH_2{=}C^{\bullet}H \quad (16)$$

The elimination of γ-OH/β-OH-group and abstraction of terminal O-bound H atom for ***RA1*** appears to be much more feasible—in both cases leading to the same O-centered radical ***A4*** product-set (eq 17).

Direct dehydration of ***RA1*** adduct (eq 17) can occur via a unique *roaming* channel (*ch*VI) initially identified for the model OH + AA reaction.[88]

$$\textbf{\textit{RA1}} \rightarrow HOPhCH{=}CHCH_2O^{\bullet}\ (\textbf{\textit{A4}}) + H_2O \quad (17)$$

A4 is a key oxygen-centered radical intermediate also identified in a previous study[55] derived from the reaction of H + *p*-CMA; thus, the notation is preserved here along with the ***A4*** notation, for comparisons. Dehydration process (*ch*VI) occurs via fairly low-energy transition states ***TSa5*** (Figure 2). The barrier height of 25.54 kcal/mol for *p*-CMA reaction (Figure 2) is below the entrance channel (by 1.73 kcal/mol). These favorable conditions are due to one of the primary roaming TS features of a loose TS structure (cf. Figure.S1). The same roaming features attributed to the OH + AA reaction are seen here as well.[88,93−96] In this case for ***TSa5***, the OH bond to the C7-carbon atom is almost broken (distance of 3.31 Å).

Transition states for roaming and direct H-abstraction from OH + *p*-CMA are very similar and located close to each other. While the imaginary frequency at ***TSa5*** is high (−1525.2 cm^{-1}) at the ωB97XD-level indicating on the similarity to the direct H-abstraction reaction, IRC analysis clearly demon-

DOI: 10.1021/acs.jpca.9b00185
J. Phys. Chem. A XXXX, XXX, XXX−XXX

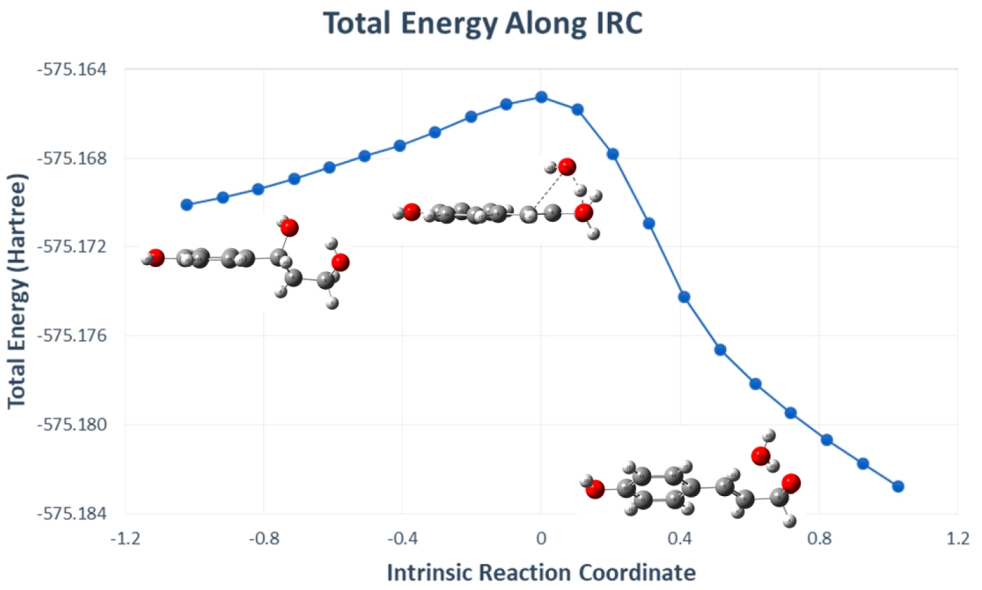

Figure 5. Roaming−like dehydration pathway for 1,3-diol radical-adduct of the chemical activation reaction OH + *p*-CMA via ***TSa5*** (see Scheme 1 and Figure 2).

strates that the roaming stationary point connects dehydration products with 1,3-diol radical adduct (***1,3-DR***) as a reagent—not the isolated OH + *p*-CMA (Figure 5). This suggests that the chemically activated ***1,3-DR*** can easily undergo a low-energy roaming dehydration to form the key radical-product ***A4*** (eq 17).

It is important to note that more suitable for exploration of VdW-regions DFT methods, such as UB97D3(BJ) functional including D3-version of Grimm's dispersion correction and Becke−Johnson dumping (recommended in ref 88 for roaming analysis in diol radicals), and even traditional UMP2 *ab initio* method well reproduce the same saddle point (***TSa5***) with even more clear roaming features, *viz.,* the typically low imaginary frequency along the minimum energy path (see Figure S1, Supporting Information). See also the supporting materials in ref 88 for a methodological overview on the roaming in the model reaction OH + AA.

Note also that reaction 17 is the more affordable channel to form ***A4*** radical than from ***RB1*** through ***TSb5*** or another roaming-like ***TSb8*** (*ch*XIII). These latter barrier heights are 44.19 and 40.15 kcal/mol, respectively, which are in excess of 14 kcal/mol higher than that through ***TSa5***.

Loss of a H atom from C_γ in ***A4*** radical generates HOPhCHCHCHO (***A5***) as seen in eq 18. From the dissociation limit, the energy barrier is 15.47 kcal/mol with a resulting energy that is 3.14 kcal/mol below the entrance channel.

A4 could also generate formaldehyde and HOPhCHC$^\bullet$H (***A6***) in eq 19, which is 5.44 kcal/mol above the entrance channel through ***TSa6*** with a 25.69 kcal/mol barrier.

$$\text{HOPhCH=CHCH}_2\text{O}^\bullet\ (\textbf{\textit{A4}}) \rightarrow \text{HOPhCHCHCHO}\ (\textbf{\textit{A5}}) + {}^\bullet\text{H} \quad (18)$$

$$\text{HOPhCH=CHCH}_2\text{O}^\bullet\ (\textbf{\textit{A4}}) \rightarrow \text{HOPhCHC}^\bullet\text{H}\ (\textbf{\textit{A6}}) + \text{CH}_2\text{O} \quad (19)$$

The dominant formation of *p*-coumaryl aldehyde and cinnamaldehyde at low temperatures (for CnA as low as 400 °C[56]) observed in our *experiments*[56,57] supports low-barrier formation of the ***A4*** radical and basically the possibility of the roaming channel. The monomer-aldehydes have been major products also in experiments by Akazawa on pyrolysis of four phenylpropanols, including *p*-CMA and CnA at 600 °C,[59] as well as by Kawamoto et al. for coniferyl alcohol, at typical for lignin pyrolysis conditions (temperature range 200−400 °C[22]).[53] Channels suggested by us (primarily roaming) are essential for the formation of cinnamaldehyde, since concerted dehydrogenation is a high-energy demanding process with an activation barrier as high as 79 kcal/mol.[56]

Although not explicitly shown in Figure 2, decomposition of the ***A4*** radical can also form the same ***A7*** product sets (eq 20) as HOPhCH(O$^\bullet$)CH=CH$_2$ (***A8***) (eq 15). Cleavage of the C1−C7 bond followed by a hydrogen transfer from C9 to C7 would generate ***A7*** and acrolein.

$$\text{HOPhCH = CHCH}_2\text{O}^\bullet\ (\textbf{\textit{A4}}) \rightarrow \text{HOPh}^\bullet\ (\textbf{\textit{A7}}) + \text{CH}_2\text{=CHCHO} \quad (20)$$

As noted above, two dehydration channels (channels V and VI) are also identified for energized ***RA1*** radical-adduct involving both hydroxy groups and leading to the conventional (***TSa7***) and roaming (***TSa5***) pathways, respectively. The conventional *ch*V, with a barrier of 35.89 kcal/mol, forms HOPhCH(O$^\bullet$)CH=CH$_2$ (***A8***) radical. The tight structure of ***TSa7*** (cf. Figure 4) explains why such a conventional transition state produces such a high energy barrier of 35.89 kcal/mol, almost 9 kcal/mol above the entrance channel, compared to the barrier for the roaming transition state in ***TSa5*** (*ch*VI) with a smaller barrier height of 25.54 kcal/mol. This occurrence is analogous to what is shown in the OH + AA reaction.[88] ***RA1*** dehydration through *ch*V forming ***A7*** can also explain the high phenol content in the low-temperature products of the *p*-CMA pyrolysis.[55]

Dehydration of ***RB1*** involving two vicinal OH-groups (channels VIII and XIII) is not straightforward, which is in accordance with AA.[88] The roaming transition state for dehydration can be difficult to optimize due to the small TS-

DOI: 10.1021/acs.jpca.9b00185
J. Phys. Chem. A XXXX, XXX, XXX−XXX

Scheme 2. Migration of the Terminal γ-OH Group (a) and Migration Followed by Splitting of the γ-OH Group over the *ortho*- and *ipso*-Ring-Centers (b)[a]

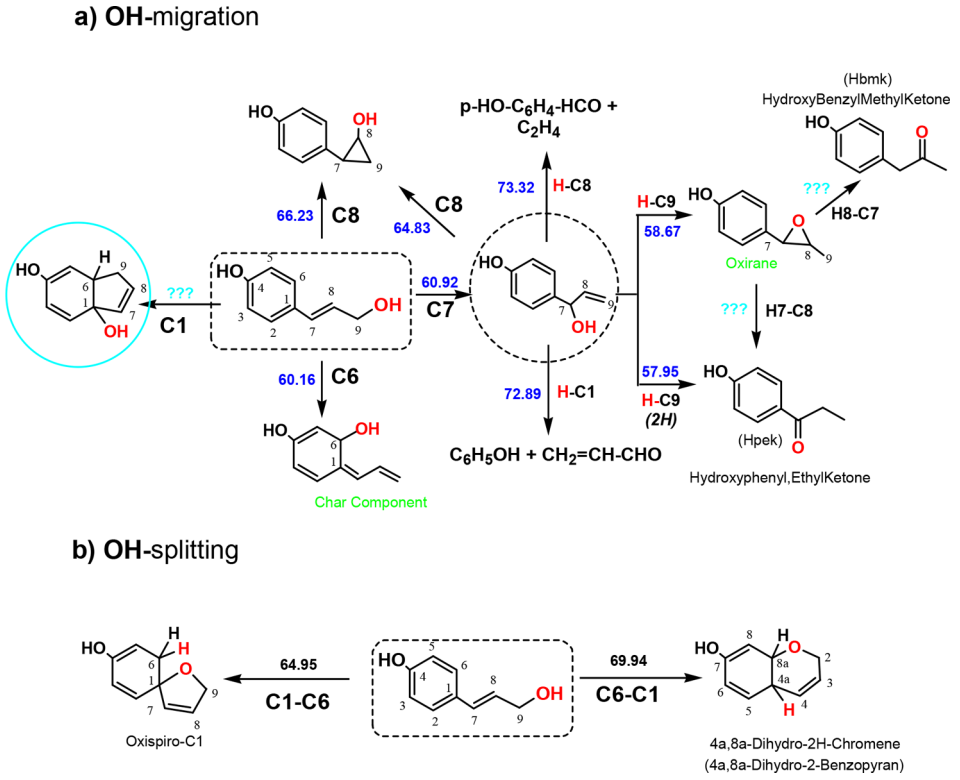

[a]The split atoms of the γ-OH moiety are highlighted in red for clarity.

ring involving vicinal (two neighboring C atoms) OH-groups such as with ***RB1***. The distance of the OH groups in the ***RB1*** adduct allows for transition states such as ***TSa5*** easier to locate.

It was possible to determine both a conventional (***TSb5***) and roaming (***TSb8***) transition state for the formation of the ***A4*** radical and water from the ***RB1*** radical (*ch*XIII and eq 21). As seen in the Figure 3 energy diagram and the structures in Figure 4, the conventional ***TSb5*** has a five-member cyclic ring created from the β-OH group attachment at C_β and the simultaneous initiation of hydrogen atom transfer from the γ-OH group. This TS produces an energy 4.53 kcal/mol above the entrance channel and a corresponding energy barrier of 44.19 kcal/mol for ***RB1*** dehydration. In comparison, the roaming ***TSb8*** structure has a lower energy barrier of 40.15 kcal/mol, 0.49 kcal/mol above the entrance channel, from a linear H atom abstraction by the OH radical.

$$\textbf{\textit{RB1}} \rightarrow \text{HOPhCH=CHCH}_2\text{O}^\bullet\ (\textbf{\textit{A4}}) + \text{H}_2\text{O} \qquad (21)$$

3.1.5. Dehydration Involving Skeletal H-Atoms. Generally, the formation of various isomers of $\text{HOPhCH}^\bullet\text{C(=O)CH}_3$ (***B5***) allylic radical could be expected bearing an OH-group located in different side-chain sites depending on the types of OH- and H-moieties are involved. However, the 5-membered ring TS reactions could not be located since the planar allylic moiety prevents such H-transfers (see also ref 42).

As also expected, the barriers for reactions involving smaller four-membered TS-rings are high. Water elimination mediated by the terminal OH-group in ***RB1*** radical (***1,2-DR***) and β-skeletal H atom, indeed, requires 67.67 kcal/mol to form $\text{HOPhCH}^\bullet\text{C(=O)CH}_3$ (***B5***) allylic radical, which is 28.0 kcal/mol higher than the entrance channel (*ch*VIII).

3.1.6. Formation of Bicyclic Products through Loss of OH-Groups and H-Atoms. These reactions involve generating bicyclic products including highly reactive epoxide or oxetane. The reactive oxygen radical created can then react with a radical center on a nearby carbon atom to form a cyclic structure. The calculated barriers for these reactions are all above 40 kcal/mol.

As seen in eqs 22 and 23, a strained epoxide, ***B7***, can be formed from both ***RA1*** (*ch*XIV) and ***RB1*** (*ch*XII) through β-H atom dissociation from the α/β-OH group over barriers of 40.57 and 52.96 kcal/mol respectfully. The difference is energies here is due to the difference in the ***RA1*** and ***RB1*** relative energies where formation of ***B7*** is 13.30 kcal/mol above the entrance channel.

$$\textbf{\textit{RA1}} \rightarrow \text{HOPhCH(cycO)CHCH}_2\text{OH}\ (\textbf{\textit{B7}}) + {}^\bullet\text{H} \qquad (22)$$

$$\textbf{\textit{RB1}} \rightarrow \text{HOPhCH(cycO)CHCH}_2\text{OH}\ (\textbf{\textit{B7}}) + {}^\bullet\text{H} \qquad (23)$$

A second strained epoxide can also be formed from ***RA1*** over a slightly higher barrier energy of 44.51 kcal/mol (*ch*IX). The products formed, eq 24, are HOPhCH(OH)CH(cycO) (***A10***) and H atom where the H atom from the γ-OH of ***RA1*** is lost leading to ring formation of the oxygen radical bonding with the C_β.

$$\textbf{\textit{RA1}} \rightarrow \text{HOPhCH(OH)CH(cycO)}\ (\textbf{\textit{A10}}) + {}^\bullet\text{H} \qquad (24)$$

Isomerization and dehydration of ***RB1*** has previously been discussed. This radical can also undergo γ-OH radical removal, *ch*VII, which involves a larger energy barrier of 51.79 kcal/mol

DOI: 10.1021/acs.jpca.9b00185
J. Phys. Chem. A XXXX, XXX, XXX−XXX

(eq 25). The lengthening of the C_γ−OH bond creates instability for C_γ which can simultaneous be stabilized through cyclization of this carbon atom with the C_α atom. Additional cyclic products can be created through similar stabilizations.

$$\textbf{\textit{RB1}} \rightarrow \text{HOPhC(cyc−OH) (}\textbf{\textit{B8}}\text{)} + {}^{\bullet}\text{OH} \quad (25)$$

As seen in Figure 4, the ***TSb6*** structure is cyclic and more of the "conventional" type of transition state (similar to ***TSa7*** previously described). The products formed, HOPhC(cyc−OH) (***B8***) and OH radical, are 8.21 kcal/mol above the energy of the free reagents. A roaming type TS, as seen with ***TSa5***, was difficult to converge on due to the proximity of the OH-groups and formation of the strained small-size structure of TS.

In the ***RB1*** radical, removal of the H atom on the γ-OH group with subsequent bonding to the C_α generates a larger HOPhCH(cycOC)OH (***B6***) oxetane four-member cyclic structure (eq 26). Although ***B6*** has a larger cyclic ring compared to the epoxide formed in from loss of the same γ-H atom, ***A10*** (eq 24) above, the energy barrier is significantly higher at 52.33 kcal/mol compared to 44.51 kcal/mol.

$$\textbf{\textit{RB1}} \rightarrow \text{HOPhCH(cycOC)OH (}\textbf{\textit{B6}}\text{)} + {}^{\bullet}\text{H} \quad (26)$$

3.2. Some Unimolecular Decomposition Channels for p-CMA. Formation of the Bicyclic Products. The OH-migration and OH-splitting can serve as the unimolecular decomposition channels for *p*-CMA, with interesting outcomes. Previously, we have theoretically identified several unimolecular decomposition pathways on the ground state PES of the *p*-CMA and its simpler model CnA (with no phenolic OH present) leading to the experimentally detected set of products in different pyrolysis conditions (conventional pyrolysis for CnA, and fractional pyrolysis for *p*-CMA).[55−57] Here we provide results on two addition types of unimolecular decomposition pathways starting from OH-migration and its splitting over the carbon backbone. For consistency, these channels were also calculated at the same B3PW91/6-31+G(2d,p) DFT level of theory as in ref 55.

For the CnA, it was established that the calculated molecular pathways are mostly higher-energy demanding processes and can be afforded only at elevated temperatures. However, due to the significant entropy gains from the fragmentation of molecules, such unimolecular decomposition channels can principally account for the formation of some experimentally observed primary products at higher temperatures.

Some reaction channels were unique and are being suggested for the first time. They were relevant not only to the biomass degradation processes, but also can represent a more general model, such as for the pathway via a biradical intermediate (Scheme 2).

Now we have identified some new reaction pathways triggered by migration of the terminal OH-group, which are also interesting.

3.2.1. γ-OH-Migration. The migration of OH-group in free radicals is a known mechanism relevant to the enzymatic[121] and atmospheric processes,[122] as well as for combustion of hydrocarbons.[123,124] Such a mechanism was identified in current work relevant to the lignin pyrolysis and thermal decomposition of its models. We have identified *four* realistic channels (for molecular *p*-CMA) involving γ-OH migration pathways, illustrated in Scheme 2. Some of these pathways have been identified previously for CnA pyrolysis.[56]

The migration of γ-OH to C_α faces ca. 61 kcal/mol barrier of activation to form 2-HPPh (encircled for clarity). Even though these isomerization pathways have similar energy requirements when compared to the molecular decomposition and homolytic bond cleavage channels, they are less competitive due to the significant entropy gain in the latter processes.

3.2.2. 1,2- and 1,3-Sigmatropic OH-shift. An epoxidation occurs after an H-transfer to C9 to form 1-methyl-2-hydroxyphenyl-oxirane (Scheme 2). This is in line with the hypothesized (particularly, by Brežný et al.[25]) formation of the *oxirane* and *oxetane* units (3- and 4-membered epoxides) during the experiments on lignin pyrolysis (see also refs 55 and 56).

3.2.3. γ-O−H Bond Splitting over the Ring and Formation of Bicyclic Products. These reactions start from the attack (more precisely, the migration since they are far from each other) of the γ-OH (*viz.*, γ-oxygen atom) group of the side-chain either to *ipso*-C1 or *ortho*-C2 ring centers followed by splitting of the γ-O−H bond over the ring, which results in the formation of the bicyclic compounds (second ring-closure via splitting of the O−H bond over these two adjacent ring centers). The transition state structures are depicted in Scheme 2b. The barrier for activation for chromene formation is substantially higher than that for *spiro*-cyclization (69.94 kcal/mol vs 64.95 kcal/mol, respectively). Such a splitting can be a straightforward mechanism for formation of intermediates identified in lignin pyrolysis, such as chromene derivatives and *oxi-spirocyclic* compounds.[125] Importantly, the *oxi*-spirocyclic moieties have been identified also as lignin structural units. Perhaps, those identified on PES *p*-CMA intermediates can also be involved in biocatalytic generation of lignins, to be responsible also for various environmental transformations. The terminal OH-splitting can serve as a molecular mechanism for enzymatic generation of the significant spirocyclic linkages in lignin.[125] We are not aware of any reports in literature on identification of such a mechanism. We confirm it here as of a new one with important outcomes.

Note that formation of the *oxiranes* and oxetanes has been hypothesized for lignin pyrolysis experiments (in particular, by Brežný et al.[25])

In our fractional pyrolysis experiments reported in ref 55, we have observed also noticeable amounts of benzofuran (BF) derivatives as well as some bis-compounds as stable products. Formation of BF can be attributed to the processes initiated by H-transfer reactions, if they are to be formed via molecular (concerted or bridged by intermediates) mechanisms.

3.3. Formation of van der Waals (VdW) Complexes. Formation of VdW-complexes are optimal situations for OH radicals to interact with target species for periods of time allowing for H atom abstraction creating a *p*-CMA radical and water. Previously, for OH + AA, we determined that the flatness of the PES regions, coupled with these VdW complexes, created situations that facilitated roaming dissociation.

Transition states involving hydrogen abstraction from OH radical were calculated with relative barrier heights shown in Scheme 3.

Pathways involving abstractions from the OH phenolic group and the Cγ atom have negative barriers characteristic of scenarios where prereaction complexes are formed. These prereaction complexes involve VdW forces which stabilize and lower the energies before the reaction takes place. This is similar to what was observed in the model AA + OH reaction. These two locations also provide the greatest stabilization upon H atom abstraction and radical formation seen in −36.23

DOI: 10.1021/acs.jpca.9b00185
J. Phys. Chem. A XXXX, XXX, XXX−XXX

Scheme 3. Hydrogen Abstraction via OH Radical Pathways in *p*-CMA, Calculated at the ωB97XD/def2TZVP Level[a]

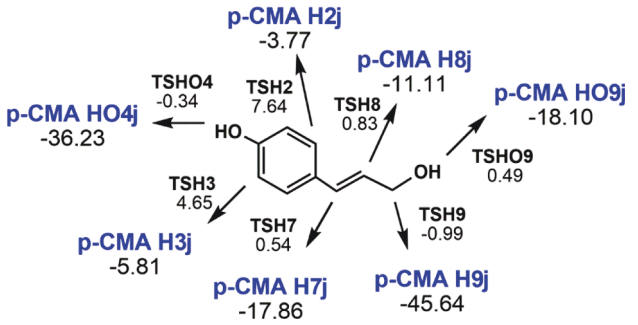

[a]Data on arrows represent corresponding relative barrier heights (ZPE-corrected electronic energies) in kcal/mol.

and −45.64 kcal/mol energy level decreases. These decreases are lower than the well depths seen for ***RA1*** and ***RB1*** radical formation of −27.27 and −39.66 kcal/mol in Figures 2 and 3.

Additional abstraction sites at C_α, C_β, and γ-OH have energy barriers below 1 kcal/mol with energy decreases ranging from 12 to 18 kcal/mol upon radical formation. Abstraction directly from the phenol ring at position C3 (or C5) has a 4.65 kcal/mol energy barrier while position C2 (or C6) is 7.64 kcal/mol showing radical formation in the conjugated ring is extremely unfavorable.

4. CONCLUSIONS

The hydroxyl-radical-initiated processes are important in pyrolysis of lignin and its fractionated intermediates. *p*-Coumaryl alcohol (*p*-CMA) is the simplest lignin precursor and structural model of the lignin end-groups containing a propanoid side-chain and phenolic OH-group, and its thermal decomposition including reactions with OH-radicals can shed a light into the thermolysis mechanisms of the intricate lignin macromolecules; to explain, in particular, the alkylation of monophenols produced during lignin pyrolysis.

A detailed PES analysis of the PES for OH + *p*-CMA reaction system is provided in this paper to study the mechanisms of the OH + *p*-CMA reactions using various DFT and *ab initio* protocols.

Several OH-addition−elimination (isomerization) channels are explored involving chemically activated (energized) adducts. In particular, various dehydration pathways are identified including the ones via high energy conventional (tight) TS (*ch*V), and its counterpart via the low-energy roaming-like saddle point (*ch*VI) with typical roaming features (loose structures, the energies below the reagents asymptote, etc.). Similarly, two different transition states, roaming and conventional for *ch*XIII were also determined for water elimination from ***RB1***. This allows suggesting a new mechanism for thermal dehydration of energized adduct-radicals during reaction of OH radicals with *p*-CMA, as it occurs with allyl alcohol as a simplest relevant model of the unsaturated alcohols. These results particularly involve dehydration to aldehydes for certain diols and support the possibility of the roaming-like mechanism in reactions of OH + unsaturated alcohols, similar to what occurs in OH + C_2H_4[97] and OH + AA[88] reactions, as well as some larger molecules.[99,100] Intriguingly, the 1,3-diol radicals containing separated OH-groups mostly undergo roaming dehydration, which contrasts with the vicinal and geminal diols, which are known to be dehydrated also enzymatically[121] and in the processes in liquids.[126]

A number of unimolecular degradation pathways are identified for the *p*-CMA molecule involving the primary products formation from bonds homolysis, followed by secondary decomposition of products. An intriguing pathway is the formation of bicyclic compounds ubiquitous in lignin chemistry via attack of the terminal OH-group *"all the way down"* along the carbon backbone to the benzene ring through splitting over the *ipso*- and *ortho*-carbon atoms of the ring.

■ ASSOCIATED CONTENT

Supporting Information

The Supporting Information is available free of charge on the ACS Publications website at DOI: 10.1021/acs.jpca.9b00185.

Optimized structures, vibrational frequencies, moments of inertia, complete references, and roaming transition state (***TSa5***) geometry (PDF)

■ AUTHOR INFORMATION

Corresponding Author

*(R.A.) E-mail: rubikasa@buffalo.edu.

ORCID

Rubik Asatryan: 0000-0003-1200-2727
Joseph W. Bozzelli: 0000-0003-4822-150X
Lavrent Khachatryan: 0000-0002-8067-7964
Eli Ruckenstein: 0000-0001-5192-4922

Notes

The authors declare no competing financial interest.

[⊥]Part II of this paper will include a detailed kinetics analysis.

■ ACKNOWLEDGMENTS

This work is partly funded by National Science Foundation under Grant CBET 1330311. R.A. acknowledges the Ruckenstein Fund at the University at Buffalo (UB) for continuous support. Computing time on the high-performance computing infrastructure "rush" was provided by the UB Center for Computational Research and the NJIT Advanced Research Computing (ARC) center.

■ REFERENCES

(1) Huber, G. W.; Iborra, S.; Corma, A. Synthesis of Transportation Fuels from Biomass: Chemistry, Catalysts, and Engineering. *Chem. Rev.* **2006**, *106*, 4044−4098.

(2) Sluiter, J. B.; Ruiz, R. O.; Scarlata, C. J.; Sluiter, A. D.; Templeton, D. W. Compositional Analysis of Lignocellulosic Feedstocks. 1. Review and Description of Methods. *J. Agric. Food Chem.* **2010**, *58*, 9043−9053.

(3) Zakzeski, J.; Bruijnincx, P. C. A.; Jongerius, A. L.; Weckhuysen, B. M. The Catalytic Valorization of Lignin for the Production of Renewable Chemicals. *Chem. Rev.* **2010**, *110*, 3552−3599.

(4) Davin, L. B.; Patten, A. M.; Jourdes, M.; Lewis, N. G. Lignins: A Twenty-First Century Challenge. *Biomass Recalcitrance: Deconstructing the Plant Cell Wall for Bioenergy* **2008**, 213−305.

(5) Azadi, P.; Inderwildi, O. R.; Farnood, R.; King, D. A. Liquid Fuels, Hydrogen and Chemicals from Lignin: A Critical Review. *Renewable Sustainable Energy Rev.* **2013**, *21*, 506−523.

(6) Ragauskas, A. J.; Beckham, G. T.; Biddy, M. J.; Chandra, R.; Chen, F.; Davis, M. F.; Davison, B. H.; Dixon, R. A.; Gilna, P.; Keller, M. Lignin Valorization: Improving Lignin Processing in the Biorefinery. *Science* **2014**, *344*, 1246843.

DOI: 10.1021/acs.jpca.9b00185
J. Phys. Chem. A XXXX, XXX, XXX−XXX

(7) Kibet, J.; Khachatryan, L.; Dellinger, B. Molecular Products and Radicals from Pyrolysis of Lignin. *Environ. Sci. Technol.* **2012**, *46*, 12994−13001.
(8) Heitner, C.; Dimmel, D. R.; Schmidt, J. A. *Lignin and Lignans: Advances in Chemistry*; 2010.
(9) Jung, H.-J. G.; Ralph, J. Phenolic−carbohydrate complexes in plant cell walls and their effect on lignocellulose utilization. In *Microbial and Plant Opportunities to Improve Lignocellulose Utilization by Ruminants*; Akin, D. E., Ed.; Elsevier Sciences: New York, 1990; pp 173−182.
(10) Kim, K. H.; Bai, X.; Cady, S.; Gable, P.; Brown, R. C. Quantitative Investigation of Free Radicals in Bio-Oil and their Potential Role in Condensed-Phase Polymerization. *ChemSusChem* **2015**, *8*, 894−900.
(11) Liao, S.; Pan, B.; Li, H.; Zhang, D.; Xing, B. Detecting Free Radicals in Biochars and Determining Their Ability to Inhibit the Germination and Growth of Corn, Wheat and Rice Seedlings. *Environ. Sci. Technol.* **2014**, *48*, 8581−8587.
(12) SriBala, G.; Carstensen, H. H.; Van Geem, K. M.; Marin, G. B. Measuring Biomass Fast Pyrolysis Kinetics: State of the Art. *Wiley Interdiscip. Rev. Energy Environ.* **2019**, *8*, e326.
(13) Joffres, B.; Laurenti, D.; Charon, N.; Daudin, A.; Quignard, A.; Geantet, C. Thermochemical Conversion of Lignin for Fuels and Chemicals: A Review. *Oil Gas Sci. Technol.* **2013**, *68*, 753−763.
(14) Khachatryan, L.; Barekati-Goudarzi, M.; Kekejian, D.; Aguilar, G.; Asatryan, R.; Stanley, G. G.; Boldor, D. Pyrolysis of Lignin in Gas-Phase Isothermal and cw-CO_2 Laser Powered Non-Isothermal Reactors. *Energy Fuels* **2018**, *32*, 12597−12606.
(15) Bährle, C.; Custodis, V.; Jeschke, G.; Van Bokhoven, J. A.; Vogel, F. In Situ Observation of Radicals and Molecular Products During Lignin Pyrolysis. *ChemSusChem* **2014**, *7*, 2022−2029.
(16) Kim, K. H.; Bai, X.; Brown, R. C. Pyrolysis Mechanisms of Methoxy Substituted α-O-4 Lignin Dimeric Model Compounds and Detection of Free Radicals Using Electron Paramagnetic Resonance Analysis. *J. Anal. Appl. Pyrolysis* **2014**, *110*, 254−263.
(17) Pandey, M. P.; Kim, C. S. Lignin Depolymerization and Conversion: A Review of Thermochemical Methods. *Chem. Eng. Technol.* **2011**, *34*, 29−41.
(18) Evans, R. J.; Milne, T. A. Molecular Characterization of the Pyrolysis of Biomass. *Energy Fuels* **1987**, *1*, 123−137.
(19) Amen-Chen, C.; Pakdel, H.; Roy, C. Production of Monomeric Phenols by Thermochemical Conversion of Biomass: A Review. *Bioresour. Technol.* **2001**, *79*, 277−299.
(20) Simon, J. P.; Eriksson, K.-E. L. The Significance of Intramolecular Hydrogen Bonding in the β-O-4 Linkage of Lignin. *J. Mol. Struct.* **1996**, *384*, 1−7.
(21) Sazanov, Y. N.; Gribanov, A. V. Thermochemistry of Lignin. *Russ. J. Appl. Chem.* **2010**, *83*, 175−194.
(22) Kawamoto, H. Lignin Pyrolysis Reactions. *J. Wood Sci.* **2017**, *63*, 117−132.
(23) Saiz-Jimenez, C.; De Leeuw, J. W. Lignin Pyrolysis Products: Their Structures and Their Significance as Biomarkers. *Org. Geochem.* **1986**, *10*, 869−876.
(24) Domburg, G.; Rossinskaya, G.; Sergseva, V. Study of Thermal Stability of β-Ether Bonds in Lignin and its Models. *Therm. Anal. Proc. Int. Conf., 4th, Budapest* 1974; Vol. 2.
(25) Brežný, R.; Mihalov, V.; Kováčik, V. Low Temperature Thermolysis of Lignins. I. Reactions of β-O-4 Model Compounds. *Holzforschung* **1983**, *37*, 199−204.
(26) Klein, M. T.; Virk, P. S. Model Pathways in Lignin Thermolysis. 1. Phenethyl Phenyl Ether. *Ind. Eng. Chem. Fundam.* **1983**, *22*, 35−45.
(27) Elder, T.; Beste, A. Density Functional Theory Study of the Concerted Pyrolysis Mechanism for Lignin Models. *Energy Fuels* **2014**, *28*, 5229−5235.
(28) Kleinert, M.; Barth, T. Phenols from Lignin. *Chem. Eng. Technol.* **2008**, *31*, 736−745.
(29) Jarvis, M. W.; Daily, J. W.; Carstensen, H. H.; Dean, A. M.; Sharma, S.; Dayton, D. C.; Robichaud, D. J.; Nimlos, M. R. Direct Detection of Products from the Pyrolysis of 2-Phenethyl Phenyl Ether. *J. Phys. Chem. A* **2011**, *115*, 428−438.
(30) Beste, A.; Buchanan, A. C., III Computational Investigation of the Pyrolysis Product Selectivity for α-Hydroxy Phenethyl Phenyl Ether and Phenethyl Phenyl Ether: Analysis of Substituent Effects and Reactant Conformer Selection. *J. Phys. Chem. A* **2013**, *117*, 3235−3242.
(31) Beste, A.; Buchanan, A. C. Challenges in the Computation of Rate Constants for Lignin Model Compounds. *Rate Constant Calculation for Thermal Reactions: Methods and Applications* **2011**, 191−238.
(32) Beste, A.; Buchanan, A. C. Role of Carbon-Carbon Phenyl Migration in the Pyrolysis Mechanism of β-O-4 Lignin Model Compounds: Phenethyl Phenyl Ether and α-Hydroxy Phenethyl Phenyl Ether. *J. Phys. Chem. A* **2012**, *116*, 12242−12248.
(33) Beste, A.; Buchanan, A. C., III Kinetic Simulation of the Thermal Degradation of Phenethyl Phenyl Ether, A Model Compound for the β-O-4 Linkage in Lignin. *Chem. Phys. Lett.* **2012**, *550*, 19−24.
(34) Younker, J. M.; Beste, A.; Buchanan, A. C., III Computational Study of Bond Dissociation Enthalpies for Substituted β-O-4 Lignin Model Compounds. *ChemPhysChem* **2011**, *12*, 3556−3565.
(35) Choi, Y. S.; Singh, R.; Zhang, J.; Balasubramanian, G.; Sturgeon, M. R.; Katahira, R.; Chupka, G.; Beckham, G. T.; Shanks, B. H. Pyrolysis Reaction Networks for Lignin Model Compounds: Unraveling Thermal Deconstruction of β-O-4 and α-O-4 Compounds. *Green Chem.* **2016**, *18*, 1762−1773.
(36) Watanabe, T.; Kawamoto, H.; Saka, S. Pyrolytic Reactivities of Deuterated β-Ether-Type Lignin Model Dimers. *J. Anal. Appl. Pyrolysis* **2015**, *112*, 23−28.
(37) Kawamoto, H.; Nakamura, T.; Saka, S. Pyrolytic Cleavage Mechanisms of Lignin-Ether Linkages: A Study on p-Substituted Dimers and Trimers. *Holzforschung* **2008**, *62*, 50−56.
(38) De Bruycker, R.; Herbinet, O.; Carstensen, H. H.; Battin-Leclerc, F.; Van Geem, K. M. Understanding the Reactivity of Unsaturated Alcohols: Experimental and Kinetic Modeling Study of the Pyrolysis and Oxidation of 3-Methyl-2-Butenol and 3-Methyl-3-Butenol. *Combust. Flame* **2016**, *171*, 237−251.
(39) Jiang, X.; Lu, Q.; Hu, B.; Liu, J.; Dong, C.; Yang, Y. A Comprehensive Study on Pyrolysis Mechanism of Substituted β-O-4 Type Lignin Dimers. *Int. J. Mol. Sci.* **2017**, *18*, 2364.
(40) Kawamoto, H.; Ryoritani, M.; Saka, S. Different Pyrolytic Cleavage Mechanisms of β-Ether Bond Depending on the Side-Chain Structure of Lignin Dimers. *J. Anal. Appl. Pyrolysis* **2008**, *81*, 88−94.
(41) Hosoya, T.; Kawamoto, H.; Saka, S. Role of Methoxyl Group in Char Formation from Lignin-Related Compounds. *J. Anal. Appl. Pyrolysis* **2009**, *84*, 79−83.
(42) Kawamoto, H.; Horigoshi, S.; Saka, S. Effects of Side-Chain Hydroxyl Groups on Pyrolytic β-Ether Cleavage of Phenolic Lignin Model Dimer. *J. Wood Sci.* **2007**, *53*, 268−271.
(43) He, T.; Zhang, Y.; Zhu, Y.; Wen, W.; Pan, Y.; Wu, J.; Wu, J. Pyrolysis Mechanism Study of Lignin Model Compounds by Synchrotron Vacuum Ultraviolet Photoionization Mass Spectrometry. *Energy Fuels* **2016**, *30*, 2204−2208.
(44) Liu, C.; Deng, Y.; Wu, S.; Mou, H.; Liang, J.; Lei, M. Study on the Pyrolysis Mechanism of Three Guaiacyl-Type Lignin Monomeric Model Compounds. *J. Anal. Appl. Pyrolysis* **2016**, *118*, 123−129.
(45) Asmadi, M.; Kawamoto, H.; Saka, S. Thermal Reactions of Guaiacol and Syringol as Lignin Model Aromatic Nuclei. *J. Anal. Appl. Pyrolysis* **2011**, *92*, 88−98.
(46) Huang, J. B.; Liu, C.; Ren, L. R.; Tong, H.; Li, W. M.; Wu, D. Studies on Pyrolysis Mechanism of Syringol as Lignin Model Compound by Quantum Chemistry. *Ranliao Huaxue Xuebao J. Fuel Chem. Technol.* **2013**, *41*, 657−666.
(47) Huang, J.; Li, X.; Wu, D.; Tong, H.; Li, W. Theoretical Studies on Pyrolysis Mechanism of Guaiacol as Lignin Model Compound. *J. Renewable Sustainable Energy* **2013**, *5*, 043112.

DOI: 10.1021/acs.jpca.9b00185
J. Phys. Chem. A XXXX, XXX, XXX−XXX

(48) Liu, C.; Zhang, Y.; Huang, X. Study of Guaiacol Pyrolysis Mechanism Based on Density Function Theory. *Fuel Process. Technol.* **2014**, *123*, 159−165.
(49) Kuroda, K. i. Pyrolysis of Arylglycol-β-Propylphenyl Ether Lignin Model in the Presence of Borosilicate Glass Fibers. I. Pyrolysis Reactions of β-Ether Compounds. *J. Anal. Appl. Pyrolysis* **1994**, *30*, 173−182.
(50) Harman-Ware, A. E.; Crocker, M.; Kaur, A. P.; Meier, M. S.; Kato, D.; Lynn, B. Pyrolysis-GC/MS of Sinapyl and Coniferyl Alcohol. *J. Anal. Appl. Pyrolysis* **2013**, *99*, 161−169.
(51) Elder, T. J.; Worley, S. D. The Application of Molecular Orbital Calculations to Wood Chemistry - The Dehydrogenation of Coniferyl Alcohol. *Wood Sci. Technol.* **1984**, *18*, 307−315.
(52) Elder, T. Coupling of Coniferyl Alcohol in the Formation of Dilignols. A Molecular Orbital Study. *Proceedings of the 8th International Conference on Wood and Pulping Chemistry, Helsinki*; 1995; Vol. *1*, pp 115−122.
(53) Kotake, T.; Kawamoto, H.; Saka, S. Pyrolysis Reactions of Coniferyl Alcohol as a Model of the Primary Structure Formed During Lignin Pyrolysis. *J. Anal. Appl. Pyrolysis* **2013**, *104*, 573−584.
(54) Kuroda, K. I. Analytical Pyrolysis Products Derived from Cinnamyl Alcohol-End Groups in Lignins. *J. Anal. Appl. Pyrolysis* **2000**, *53*, 123−134.
(55) Asatryan, R.; Bennadji, H.; Bozzelli, J. W.; Ruckenstein, E.; Khachatryan, L. Molecular Products and Fundamentally Based Reaction Pathways in the Gas-Phase Pyrolysis of the Lignin Model Compound p-Coumaryl Alcohol. *J. Phys. Chem. A* **2017**, *121*, 3352−3371.
(56) Khachatryan, L.; Xu, M. X.; Wu, A. J.; Pechagin, M.; Asatryan, R. Radicals and Molecular Products from the Gas-Phase Pyrolysis of Lignin Model Compounds. Cinnamyl Alcohol. *J. Anal. Appl. Pyrolysis* **2016**, *121*, 75−83.
(57) Xu, M. X.; Khachatryan, L.; Baev, A.; Asatryan, R. Radicals from the Gas-Phase Pyrolysis of a Lignin Model Compound: p-Coumaryl Alcohol. *RSC Adv.* **2016**, *6*, 62399−62405.
(58) Elder, T. Application of Computational Chemistry to Lignin Pyrolysis. *Abstracts of Papers of the American Chemical Society* **2010**, 239.
(59) Akazawa, M.; Kojima, Y.; Kato, Y. Pyrolysate Formation from Four Different Phenyl Propanols and Classification of the Initial Reaction Pathways. *Int. J. Renewable Energy Technology* **2015**, *4*, 1−14.
(60) Akazawa, M.; Kojima, Y.; Kato, Y. Reaction Mechanisms of Pyrolysis of Four Different Phenylpropanoids. *Pyrolysis Technol. J.* **2015**, *1*, 1−12.
(61) Furutani, Y.; Dohara, Y.; Kudo, S.; Hayashi, J. I.; Norinaga, K. Computational Study on the Thermal Decomposition of Phenol-Type Monolignols. *Int. J. Chem. Kinet.* **2018**, *50*, 304−316.
(62) Platonov, V. V.; Proskuryakov, V. A.; Ryl'tsova, S. V.; Popova, Y. N. *Russ. J. Appl. Chem.* **2001**, *74*, 1047−1052.
(63) Pecullan, M.; Brezinsky, K.; Glassman, I. Pyrolysis and Oxidation of Anisole Near 1000 K. *J. Phys. Chem. A* **1997**, *101*, 3305−3316.
(64) International Congress on Energy 2014, ICE 2014 - Topical Conference at the 2014 AIChE Annual Meeting.
(65) Arends, I. W. C. E.; Louw, R.; Mulder, P. Kinetic Study of the Thermolysis of Anisole in a Hydrogen Atmosphere. *J. Phys. Chem.* **1993**, *97*, 7914−7925.
(66) Nowakowska, M.; Herbinet, O.; Dufour, A.; Glaude, P. A. Detailed Kinetic Study of Anisole Pyrolysis and Oxidation to Understand Tar Formation During Biomass Combustion and Gasification. *Combust. Flame* **2014**, *161*, 1474−1488.
(67) Khachatryan, L.; Adounkpe, J.; Asatryan, R.; Dellinger, B. Radicals from the Gas-Phase Pyrolysis of Catechol: 1. *o*-Semiquinone and *ipso*-Catechol Radicals. *J. Phys. Chem. A* **2010**, *114*, 2306−2312.
(68) Khachatryan, L.; Asatryan, R.; McFerrin, C.; Adounkpe, J.; Dellinger, B. Radicals from the Gas-Phase Pyrolysis of Catechol. 2. Comparison of the Pyrolysis of Catechol and Hydroquinone. *J. Phys. Chem. A* **2010**, *114*, 10110−10116.
(69) Da Silva, G.; Bozzelli, J. W. Quantum Chemical Study of the Thermal Decomposition of *o*-Quinone Methide (6-Methylene-2,4-cyclohexadien-1-one). *J. Phys. Chem. A* **2007**, *111*, 7987−7994.
(70) Dorrestijn, E.; Epema, O. J.; Van Scheppingen, W. B.; Mulder, P. *o*-Quinone Methide as a Common Intermediate in the Pyrolysis of *o*-Hydroxybenzyl Alcohol, Chroman and 1,4-Benzodioxin. *J. Chem. Soc., Perkin Trans. 2* **1998**, 1173−1178.
(71) Eider, T. J.; McKee, M. L.; Worley, S. D. The Application of Molecular Orbital Calculations to Wood Chemistry. V. The Formation and Reactivity of Quinone Methide Intermediates. *Holzforschung* **1988**, *42*, 233−240.
(72) Kim, K. H.; Dutta, T.; Walter, E. D.; Isern, N. G.; Cort, J. R.; Simmons, B. A.; Singh, S. Chemoselective Methylation of Phenolic Hydroxyl Group Prevents Quinone Methide Formation and Repolymerization During Lignin Depolymerization. *ACS Sustainable Chem. Eng.* **2017**, *5*, 3913−3919.
(73) Ponomarev, D. A. Formation of Quinone Methides: An Alternative Pathway of Thermal Degradation of Some β-O-4-Ethers as Compounds Modeling Lignin. *Russ. J. Appl. Chem.* **1997**, *70*, 824−826.
(74) Shigematsu, M.; Kobayashi, T.; Taguchi, H.; Tanahashi, M. Transition State Leading to β-O′ Quinonemethide Intermediate of p-Coumaryl Alcohol Analyzed by Semi-Empirical Molecular Orbital Calculation. *J. Wood Sci.* **2006**, *52*, 128−133.
(75) Bland, J.; Da Silva, G. A Detailed Chemical Kinetic Model for Pyrolysis of the Lignin Model Compound Chroman. *AIMS Environ. Sci.* **2013**, *1*, 12−25.
(76) Asatryan, R.; Davtyan, A.; Khachatryan, L.; Dellinger, B. Theoretical Study of Open-Shell *ipso*-Addition and bis-Keto Dimer Interconversion Reactions Related to Gas-Phase Formation of PCDD/FS from Chlorinated Phenols. *Organohalogen Compd.* **2002**, *56*, 277−280.
(77) Britt, P. F.; Buchanan, A. C., III; Malcolm, E. A. Thermolysis of Phenethyl Phenyl Ether: A Model for Ether Linkages in Lignin and Low Rank Coal. *J. Org. Chem.* **1995**, *60*, 6523−6536.
(78) Britt, P. F.; Buchanan, A. C., III; Cooney, M. J.; Martineau, D. R. Flash Vacuum Pyrolysis of Methoxy-Substituted Lignin Model Compounds. *J. Org. Chem.* **2000**, *65*, 1376−1389.
(79) Chu, S.; Subrahmanyam, A. V.; Huber, G. W. The Pyrolysis Chemistry of a β-O-4 Type Oligomeric Lignin Model Compound. *Green Chem.* **2013**, *15*, 125−136.
(80) Kohl, I. E.; Asatryan, R.; Bao, H. No Oxygen Isotope Exchange Between Water and APS-Sulfate at Surface Temperature: Evidence from Quantum Chemical Modeling and Triple-Oxygen Isotope Experiments. *Geochim. Cosmochim. Acta* **2012**, *95*, 106−118.
(81) Schlosberg, R. H.; Ashe, T. R.; Pancirov, R. J.; Donaldson, M. Pyrolysis of Benzyl Ether Under Hydrogen Starvation Conditions. *Fuel* **1981**, *60*, 155−157.
(82) Schlosberg, R. H.; Davis Jr, W. H.; Ashe, T. R. Pyrolysis Studies of Organic Oxygenates. 2. Benzyl Phenyl Ether Pyrolysis Under Batch Autoclave Conditions. *Fuel* **1981**, *60*, 201−204.
(83) Pu, Y.; Hu, F.; Huang, F.; Ragauskas, A. J. Lignin Structural Alterations in Thermochemical Pretreatments with Limited Delignification. *BioEnergy Res.* **2015**, *8*, 992−1003.
(84) Korobkov, V. Y.; Grigorieva, E. N.; Bykov, V. I.; Kalechitz, I. V. Effect of the Structure of Coal-Related Model Ethers on the Rate and Mechanism of Their Thermolysis. 2. Effect of Substituents in the $C_6H_5CH_2OC_6H_4X$ structure. *Fuel* **1988**, *67*, 663−665.
(85) Korobkov, V. Y.; Grigorieva, E. N.; Bykov, V. I.; Senko, O. V.; Kalechitz, I. V. Effect of the Structure of Coal-Related Model Ethers on the Rate and Mechanism of Their Thermolysis. 1. Effect of the Number of Methylene Groups in the $R(CH_2)_nO(CH_2)_mR$ Structure. *Fuel* **1988**, *67*, 657−662.
(86) Khachatryan, L.; Adounkpe, J.; Maskos, Z.; Dellinger, B. Formation of Cyclopentadienyl Radical from the Gas-Phase Pyrolysis of Hydroquinone, Catechol, and Phenol. *Environ. Sci. Technol.* **2006**, *40*, 5071−5076.

DOI: 10.1021/acs.jpca.9b00185
J. Phys. Chem. A XXXX, XXX, XXX−XXX

(87) Zhang, Y.; Chao, K.; Sun, J.; Su, Z.; Pan, X.; Zhang, J.; Wang, R. Theoretical Study on the Gas Phase Reaction of Allyl Alcohol with Hydroxyl Radical. *J. Phys. Chem. A* **2013**, *117*, 6629−6640.
(88) Asatryan, R.; Pal, Y.; Hachmann, J.; Ruckenstein, E. Roaming-Like Mechanism for Dehydration of Diol Radicals. *J. Phys. Chem. A* **2018**, *122*, 9738−9754.
(89) Le Person, A.; Solignac, G.; Oussar, F.; Daële, V.; Mellouki, A.; Winterhalter, R.; Moortgat, G. K. Gas Phase Reaction of Allyl Alcohol (2-Propen-1-ol) with OH Radicals and Ozone. *Phys. Chem. Chem. Phys.* **2009**, *11*, 7619−7628.
(90) Orlando, J. J.; Tyndall, G. S.; Ceazan, N. Rate Coefficients and Product Yields from Reaction of OH with 1-Penten-3-ol, (Z)-2-Penten-1-ol, and Allyl Alcohol (2-Propen-1-ol). *J. Phys. Chem. A* **2001**, *105*, 3564−3569.
(91) Papagni, C.; Arey, J.; Atkinson, R. Rate Constants for the Gas-Phase Reactions of OH Radicals with a Series of Unsaturated Alcohols. *Int. J. Chem. Kinet.* **2001**, *33*, 142−147.
(92) Upadhyaya, H. P.; Kumar, A.; Naik, P. D.; Sapre, A. V.; Mittal, J. P. Kinetics of OH Radical Reaction with Allyl Alcohol (H_2C═$CHCH_2OH$) and Propargyl Alcohol ($HCCCH_2OH$) Studied by LIF. *Chem. Phys. Lett.* **2001**, *349*, 279−285.
(93) Houston, P. L.; Conte, R.; Bowman, J. M. Roaming under the Microscope: Trajectory Study of Formaldehyde Dissociation. *J. Phys. Chem. A* **2016**, *120*, 5103−5114.
(94) Bowman, J. M. Roaming. *Mol. Phys.* **2014**, *112*, 2516−2528.
(95) Bowman, J. M.; Suits, A. G. Roaming Reactions: The Third Way. *Phys. Today* **2011**, *64*, 33−37.
(96) Herath, N.; Suits, A. G. Roaming Radical Reactions. *J. Phys. Chem. Lett.* **2011**, *2*, 642−647.
(97) Kamarchik, E.; Koziol, L.; Reisler, H.; Bowman, J. M.; Krylov, A. I. Roaming Pathway Leading to Unexpected Water + Vinyl Products in C_2H_4OH Dissociation. *J. Phys. Chem. Lett.* **2010**, *1*, 3058−3065.
(98) McKown, B. G.; Ceriotti, M.; Womack, C. C.; Kamarchik, E.; Butler, L. J.; Bowman, J. M. Effects of High Angular Momentum on the Unimolecular Dissociation of CD_2CD_2OH: Theory and Comparisons with Experiment. *J. Phys. Chem. A* **2013**, *117*, 10951−10963.
(99) Tsai, P. Y.; Li, H. K.; Kasai, T.; Lin, K. C. Roaming as the Dominant Mechanism for Molecular Products in the Photodissociation of Large Aliphatic Aldehydes. *Phys. Chem. Chem. Phys.* **2015**, *17*, 23112−23120.
(100) Mereshchenko, A. S.; Butaeva, E. V.; Borin, V. A.; Eyzips, A.; Tarnovsky, A. N. Roaming-Mediated Ultrafast Isomerization of Geminal Tri-Bromides in the Gas and Liquid Phases. *Nat. Chem.* **2015**, *7*, 562.
(101) Davis, M. E.; Burkholder, J. B. Rate Coefficients for the Gas-Phase Reaction of OH with (Z)-3-Hexen-1-ol, 1-Penten-3-ol, (E)-2-Penten-1-ol, and (E)-2-Hexen-1-ol Between 243 and 404 K. *Atmos. Chem. Phys.* **2011**, *11*, 3347−3358.
(102) Cramer, C. J. *Essentials of Computational Chemistry: Theories and Models*; Wiley: New York, 2002.
(103) Chai, J. D.; Head-Gordon, M. Long-Range Corrected Hybrid Density Functionals with Damped Atom-Atom Dispersion Corrections. *Phys. Chem. Chem. Phys.* **2008**, *10*, 6615−6620.
(104) Zheng, J.; Xu, X.; Truhlar, D. G. Minimally Augmented Karlsruhe Basis Sets. *Theor. Chem. Acc.* **2011**, *128*, 295−305.
(105) Binkley, J. S.; Pople, J. A.; Hehre, W. J. Self-Consistent Molecular Orbital Methods. 21. Small Split-Valence Basis Sets for First-Row Elements. *J. Am. Chem. Soc.* **1980**, *102*, 939−947.
(106) Weigend, F.; Ahlrichs, R. Balanced Basis Sets of Split Valence, Triple Zeta Valence and Quadruple Zeta Valence Quality for H to Rn: Design and Assessment of Accuracy. *Phys. Chem. Chem. Phys.* **2005**, *7*, 3297−3305.
(107) Zhao, Y.; Truhlar, D. G. The M06 Suite of Density Functionals for Main Group Thermochemistry, Thermochemical Kinetics, Noncovalent Interactions, Excited States, and Transition Elements: Two New Functionals and Systematic Testing of Four M06-Class Functionals and 12 Other Functionals. *Theor. Chem. Acc.* **2008**, *120*, 215−241.
(108) Becke, A. D. Density-Functional Thermochemistry. III. The Role of Exact Exchange. *J. Chem. Phys.* **1993**, *98*, 5648−5652.
(109) Lee, C.; Yang, W.; Parr, R. G. Development of the Colle-Salvetti Correlation-Energy Formula into a Functional of the Electron Density. *Phys. Rev. B: Condens. Matter Mater. Phys.* **1988**, *37*, 785−789.
(110) Asatryan, R.; Bozzelli, J. W. Chain Branching and Termination in the Low-Temperature Combustion of *n*-Alkanes: 2-Pentyl Radical + O_2, Isomerization and Association of the Second O_2. *J. Phys. Chem. A* **2010**, *114*, 7693−7708.
(111) Asatryan, R.; Bozzelli, J. W.; Ruckenstein, E. Dihydrogen Catalysis: A Degradation Mechanism for N_2-Fixation Intermediates. *J. Phys. Chem. A* **2012**, *116*, 11618−11642.
(112) Asatryan, R.; Ruckenstein, E. Mechanism of Iron Carbonyl-Catalyzed Hydrogenation of Ethylene. 1. Theoretical Exploration of Molecular Pathways. *J. Phys. Chem. A* **2013**, *117*, 10912−10932.
(113) Da Silva, G.; Bozzelli, J. W.; Asatryan, R. Hydroxyl Radical Initiated Oxidation of *s*-Triazine: Hydrogen Abstraction is Faster than Hydroxyl Addition. *J. Phys. Chem. A* **2009**, *113*, 8596−8606.
(114) Matsugi, A. Roaming Dissociation of Ethyl Radicals. *J. Phys. Chem. Lett.* **2013**, *4*, 4237−4240.
(115) Asatryan, R.; Da Silva, G.; Bozzelli, J. W. Quantum Chemical Study of the Acrolein (CH_2CHCHO) + OH + O_2 Reactions. *J. Phys. Chem. A* **2010**, *114*, 8302−8311.
(116) Asatryan, R.; Ruckenstein, E. Dihydrogen Catalysis: A Remarkable Avenue in the Reactivity of Molecular Hydrogen. *Catal. Rev.: Sci. Eng.* **2014**, *56*, 403−475.
(117) Frisch, M. J.; Trucks, G. W.; Schlegel, H. B.; Scuseria, G. E.; Robb, M. A.; Cheeseman, J. R.; Scalmani, G.; Barone, V.; Petersson, G. A.; Nakatsuji, H. et al. *Gaussian 16, Revision A.03*; Gaussian, Inc.: Wallingford, CT, 2016.
(118) Albarran, G.; Schuler, R. H. Concerted Effects of Substituents in the Reaction of •OH Radicals with Aromatics: The Cresols. *J. Phys. Chem. A* **2005**, *109*, 9363−9370.
(119) Yamada, T.; Bozzelli, J. W.; Lay, T. Kinetic and Thermodynamic Analysis on OH Addition to Ethylene: Adduct Formation, Isomerization, and Isomer Dissociations. *J. Phys. Chem. A* **1999**, *103*, 7646−7655.
(120) Asatryan, R. S.; Grigoryan, S. G.; Arzumanyan, A. M.; Matnishyan, A. A. Quantum Chemical Study of the Mechanism of Radical Polymerization of Substituted Vinylacetylenes. *Polym. Sci. U.S.S.R.* **1985**, *27*, 2831−2836.
(121) Smith, D. M.; Golding, B. T.; Radom, L. Understanding the Mechanism of B_{12}-Dependent Diol Dehydratase: A Synergistic Retro-Push-Pull Proposal. *J. Am. Chem. Soc.* **2001**, *123*, 1664−1675.
(122) Asatryan, R.; Bozzelli, J. W. Formation of a Criegee Intermediate in the Low-Temperature Oxidation of Dimethyl Sulfoxide. *Phys. Chem. Chem. Phys.* **2008**, *10*, 1769−1780.
(123) Asatryan, R.; Raman, S.; Bielenberg, P. A.; Peterson, B.; Bozzelli, J. W.; Weissman, W. Fundamentally Based Mechanism for Oxidation of Iso-Octane. *Proceedings, 7th US National Combustion Meeting* 2011, *1*, 382−395.
(124) Green, W. H.; Wijaya, C. D.; Yelvington, P. E.; Sumathi, R. Predicting Chemical Kinetics with Computational Chemistry: Is QOOH → HOQO Important in Fuel Ignition? *Mol. Phys.* **2004**, *102*, 371−380.
(125) Pemba, A. G.; Rostagno, M.; Lee, T. A.; Miller, S. A. Cyclic and Spirocyclic Polyacetal Ethers from Lignin-Based Aromatics. *Polym. Chem.* **2014**, *5*, 3214−3221.
(126) Jiang, D.; Barata-Vallejo, S.; Golding, B. T.; Ferreri, C.; Chatgilialoglu, C. Revisiting the Reaction of Hydroxyl Radicals with Vicinal Diols in Water. *Org. Biomol. Chem.* **2012**, *10*, 1102−1107.

DOI: 10.1021/acs.jpca.9b00185
J. Phys. Chem. A XXXX, XXX, XXX−XXX